AGU PUBLICATIONS

Geochemistry, Geophysics, Geosystems

RESEARCH ARTICLE
10.1002/2016GC006497

The temperature of the Icelandic mantle from olivine-spinel aluminum exchange thermometry

S. Matthews[1], O. Shorttle[1,2], and J. Maclennan[1]

[1]Department of Earth Sciences, University of Cambridge, Cambridge, UK, [2]Department of Geological and Planetary Sciences, California Institute of Technology, Pasadena, California, USA

Key Points:
- Olivine-spinel aluminum exchange crystallization temperatures for Iceland are 150°C hotter than for MORB
- Variations in mantle lithology and melt source depth can cause a 200°C range in crystallization temperature at constant mantle temperature
- Crystallization temperature can be combined with melt chemistry and crustal thickness to constrain mantle potential temperature

Supporting Information:
- Supporting Information S1
- Data Set S1

Correspondence to:
S. Matthews,
sm905@cam.ac.uk

Citation:
Matthews, S., O. Shorttle, and J. Maclennan (2016), The temperature of the Icelandic mantle from olivine-spinel aluminum exchange thermometry, *Geochem. Geophys. Geosyst.*, *17*, 4725–4752, doi:10.1002/2016GC006497.

Received 21 JUN 2016
Accepted 3 NOV 2016
Accepted article online 7 NOV 2016
Published online 24 NOV 2016

Abstract New crystallization temperatures for four eruptions from the Northern Volcanic Zone of Iceland are determined using olivine-spinel aluminum exchange thermometry. Differences in the olivine crystallization temperatures between these eruptions are consistent with variable extents of cooling during fractional crystallization. However, the crystallization temperatures for Iceland are systematically offset to higher temperatures than equivalent olivine-spinel aluminum exchange crystallization temperatures published for MORB, an effect that cannot be explained by fractional crystallization. The highest observed crystallization temperature in Iceland is 1399 ± 20°C. In order to convert crystallization temperatures to mantle potential temperature, we developed a model of multilithology mantle melting that tracks the thermal evolution of the mantle during isentropic decompression melting. With this model, we explore the controls on the temperature at which primary melts begin to crystallize, as a function of source composition and the depth from which the magmas are derived. Large differences (200°C) in crystallization temperature can be generated by variations in mantle lithology, a magma's inferred depth of origin, and its thermal history. Combining this model with independent constraints on the magma volume flux and the effect of lithological heterogeneity on melt production, restricted regions of potential temperature-lithology space can be identified as consistent with the observed crystallization temperatures. Mantle potential temperature is constrained to be 1480^{+37}_{-30} °C for Iceland and 1318^{+44}_{-32} °C for MORB.

1. Introduction

The mantle's temperature controls its evolution, rheology, and the degree to which it can interact with the surface environment through tectonic and volcanic activity [e.g., *McGovern and Schubert*, 1989]. Temperature variations in the mantle drive convective circulation over wavelengths of 10^2 to 10^4 km, from small-scale convection at thermal boundary layers, through to plumes, superswells, and plates [e.g., *Hoggard et al.*, 2016]. By producing volcanism at mid-ocean ridges, ocean islands, and arcs, this convective circulation links the thermal and chemical evolution of the deep mantle to that of the oceans and atmosphere. All models of the Earth's geological past must therefore be based on understanding its thermal evolution, and the key point for calibration in these models is the mantle's present-day temperature. In this study, we will place new constraints on this parameter and its spatial variability, by calculating new temperatures for the mantle under Iceland and under the mid-ocean ridge system.

Iceland is a region of anomalous melting situated on the Mid-Atlantic Ridge, where zero-age crustal thickness is 20 km at the coasts [*Darbyshire et al.*, 2000], and rises to 40 km in central Iceland [*Darbyshire et al.*, 1998]. A number of physical and chemical factors have been invoked to explain this anomalous melt production: high mantle temperatures [e.g., *White et al.*, 1992; *Shorttle et al.*, 2014], higher melt fluxes from plume-driven upwelling [*Ito et al.*, 1999; *Maclennan et al.*, 2001; *Brown and Lesher*, 2014] and anomalously fusible mantle [*Foulger and Anderson*, 2005]. To test the relative importance of these factors in controlling the extent of melting beneath Iceland, it is critical to obtain independent observations of mantle temperature. One approach is to fit models of mantle processes to observations that are indirectly sensitive to temperature, such as crustal thickness [*Brown and Lesher*, 2014], both crustal thickness and lower crustal seismic velocity [*Korenaga et al.*, 2002; *White et al.*, 2008], bathymetry [*Ribe et al.*, 1995], major element geochemistry [*Herzberg and Asimow*, 2015; *Hole and Millet*, 2016], and trace element geochemistry [*McKenzie and O'Nions*, 1991; *Maclennan et al.*, 2001; *Shorttle et al.*, 2014]. Both lateral decreases in seismic velocity identified by

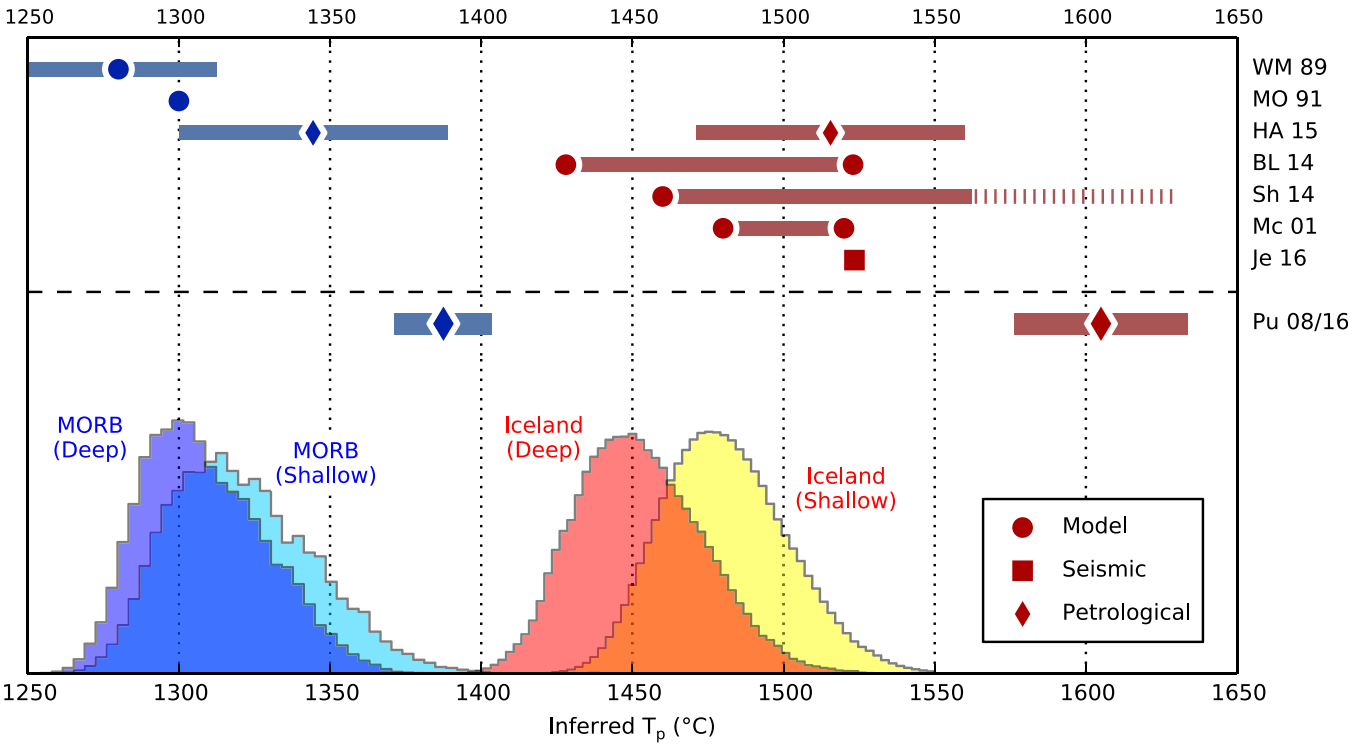

Figure 1. Comparison of previous T_p estimates for mid-ocean ridges (blue) and Iceland (orange/yellow), with the results of our T_p inversions presented here as histograms in the lower half of the figure. Estimates of T_p derived from olivine-liquid equilibration temperatures by *Putirka* [2008a, 2016] (Pu 08/16) are shown below the dashed line. The two inversion results for each setting are from the two end-member cases: maximum and minimum T_{crys} for a given T_p, corresponding to melts sourced from deep and shallow within the melting region, respectively. *Jenkins et al.* [2016] (JE 16) estimate a ΔT_p of 210°C, shown here relative to the median T_p from the MORB inversion. *Shorttle et al.* [2014] (Sh 14) report a minimum bound, represented by the point and dashed line. The other literature estimates are BL14, *Brown and Lesher* [2014]; HA 15, *Herzberg and Asimow* [2015]; Mc 01, *Maclennan et al.* [2001]; MO 91, *McKenzie and O'Nions* [1991]; and WM 89, *White and McKenzie* [1989]. Where there are two symbols a range of estimates is reported; single symbols and bars indicate a single estimate and its reported uncertainty.

tomographic inversions [*Rickers et al.*, 2013] and observations of mantle transition zone topography imaged with receiver functions [*Shen et al.*, 2002; *Jenkins et al.*, 2016] have been used to infer temperature excesses below Iceland. A third approach is to use petrological estimates of crystal-melt equilibration temperatures and calculate back from this a mantle potential temperature (T_p). In section 1.1, we review previous applications of this methodology. However, Figure 1 shows that these techniques have produced widely varying results when applied individually to estimating the temperature of the Icelandic mantle. In this manuscript, we will formally combine constraints from petrological thermometry, crustal thicknesses, and geochemistry to find a mantle temperature consistent with each independent constraint.

1.1. Petrological Temperature Estimates

Mantle potential temperature estimates based on petrological observations generally work by inferring primary magma compositions, followed either by fitting this to predicted accumulated mantle melt compositions [*Herzberg and Asimow*, 2015; *Hole and Millet*, 2016], or estimating the temperature of olivine saturation and extrapolating back to the solidus [*Putirka*, 2008a, 2016]. Differences in olivine-melt equilibration temperatures have been observed as a function of tectonic setting [*Putirka*, 2008a; *Coogan et al.*, 2014; *Heinonen et al.*, 2015; *Putirka*, 2016] and time [*Putirka*, 2016; *Spice et al.*, 2016]. However, many of these studies do not apply a correction for the cooling associated with the melting process. Such a correction is applied by *Putirka* [2005, 2008a, 2016], where absolute potential temperatures are estimated from olivine-liquid equilibration temperatures. However, a discrepancy of ~100°C exists between the potential temperature estimates reported by *Putirka* [2008a, 2016] and those based on other methods (Figure 1). A potential challenge in employing olivine-liquid equilibria to obtain mantle temperatures is that the composition of the magma in equilibrium with the most forsteritic olivine crystals must be known. In general, olivine crystals may be out of equilibrium with their carrier liquid [e.g., *Helz*, 1987; *Thomson and Maclennan*, 2013], requiring that their parental liquid composition be estimated. While this extrapolation is a straight-forward

process if only one primary magma exists for any one eruption, fractional melt extraction from the mantle can generate multiple primary melts that are not fully mixed at the time of olivine saturation [*Sobolev*, 1996; *Slater et al*., 2001]. *Keiding et al*. [2011] and *Herzberg* [2011] described how incomplete mixing of fractional melts can cause primary magma MgO and FeO concentrations to be overestimated, which propagates into higher crystallization temperature estimates.

The most forsteritic olivines found in erupted Icelandic basalts [*Maclennan et al*., 2003] and MORB basalts [*Sobolev and Shimizu*, 1994; *Sobolev*, 1996] host melt inclusions with diverse trace element and isotop geochemistries. It follows that these crystals are derived from unmixed mantle melts derived from a range of depths and source lithologies. Major element concentrations in the melts (including MgO and FeO) will also vary with melting depth and lithology, so it is likely these unmixed melts will saturate in olivine at different temperatures and with different forsterite content when crystallization proceeds at low pressure. Mantle of a single T_p can therefore give rise to primary magmas that cross their low pressure liquidii at a range of temperatures. This process may introduce considerable uncertainty into the conversion of crystallization temperatures to mantle temperature.

1.2. Methodology

Using the olivine-spinel Al-exchange thermometer [*Wan et al*., 2008; *Coogan et al*., 2014] is advantageous over olivine-liquid thermometry because it only requires assumptions about coexisting olivine and spinel being in equilibrium, rather than assumptions about equilibration pressure, or the composition of a melt that is no longer present. The crystallization temperatures estimated using the Al-exchange thermometer are lower than those estimated using olivine-liquid equilibria [*Coogan et al*., 2014]. In Appendix A, the factors contributing to this discrepancy are discussed. The discrepancy in equilibration temperatures, and consequently mantle temperature, for Iceland arise from overestimation of primary FeO by *Putirka* [2008a] due to incomplete mixing of fractional melts (Table A1). For MORB the discrepancy derives from the assumption by *Putirka* [2008a] that melt and olivine equilibrated at mantle pressures, rather than crustal pressures as done here.

The samples and analytical techniques used are described in sections 2 and 3. In section 4, we present new determinations of crystallization temperatures for four eruptions from the Northern Volcanic Zone of Iceland, and compare these to crystallization temperatures at mid-ocean ridges and estimates from elsewhere in Iceland. In section 5, we use a thermal model to calculate how mantle temperature, mantle composition and melt source depth affect crystallization temperature. By inverting this model and combining observations of crustal thickness and pyroxenite contributions to melt chemistry, we show that the Icelandic mantle is at least 140°C hotter than the MORB source mantle. In section 6, we discuss the results and the validity of our assumptions. This approach not only integrates petrological, geochemical, and geophysical observations, but additionally quantifies uncertainty arising from the trade-off between mantle temperature, composition, and melt extraction processes.

2. Samples

Figure 2 shows the location of the eruptions from which samples were analyzed. The Theistareykir picrite is an extremely olivine-rich postglacial lava flow, situated near to the northern tip of the Northern Volcanic Zone [*Elliott et al*., 1991; *Slater et al*., 2001]. Borgarhraun is an olivine, clinopyroxene-phyric, and plagioclase-phyric lava flow in the Theistareykir volcanic system [*Maclennan et al*., 2003] and is also postglacial in age [*Saemundsson*, 1991]. Both the picrite and Borgarhraun samples were collected from lava flows as whole rocks. Herubreiartögl was formed during a subglacial eruption close to the end of the last glaciation [*Werner et al*., 1996]. Samples were collected from the olivine-phyric and plagioclase-phyric pillow lavas at the north of the mountain. Kistufell is a monogenetic table mountain located at the northern margin of the Vatnajökull ice cap and most likely formed toward the end of the last glaciation [*Breddam*, 2002]. The samples were collected from the olivine-rich pillow lavas near the base of the mountain.

3. Analytical Methods

Fresh olivine crystals from Herubreiartögl and Kistufell were picked from crushed tephra and pillow glass, respectively, cleaned, mounted in resin and then polished. For the Borgarhraun and Theistareykir picrite

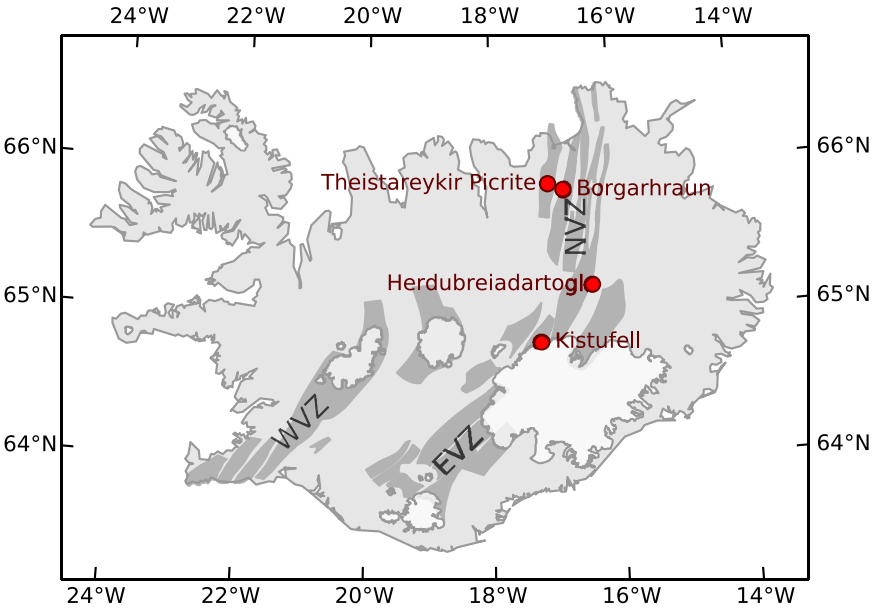

Figure 2. Map of Iceland showing the locations of the four eruptions studied, with the neovolcanic zones marked in dark grey. NVZ, EVZ, and WVZ are the Northern, Eastern, and Western Volcanic Zones, respectively.

eruptions, 30 μm thick polished sections were prepared from whole-rock samples. Olivine and spinel pairs were chosen for analysis such that the spinel was within the core of the olivine crystal. Both olivine and spinel were analyzed for Al, Cr, Fe, Mn, Ni, Si, Mg, Ca, Ti, and P with the Cameca SX-100 electron microprobe at the Department of Earth Sciences, University of Cambridge, over four sessions. Calibration was performed at the start of each session using natural and synthetic standards. An acceleration voltage of 15 kV, and currents of 40 nA for spinel and 100 nA for olivine were used. Under these conditions, the detection limit for Al in olivine was 12 ppm. A profile of points spaced ~10 μm apart was collected in each olivine crystal oriented toward the spinel inclusion and approximately perpendicular to, the nearest olivine crystal edge (Figure 3). Similarly, a profile through the diameter of each spinel inclusion with a point spacing of ~7 μm was collected in a direction parallel to the olivine profile (Figure 3). Estimates of measurement precision for each element used in the calculation were calculated from the scatter of points about their mean value in unzoned crystals. Where the uncertainty arising from this internal reproducibility is greater than the uncertainty calculated on the basis of counting statistics, it is used in preference. See supporting information Table S1 for more information.

4. Olivine-Spinel Al-Exchange Thermometry

Aluminum exchange between olivine and spinel was parameterized as a function of temperature by *Coogan et al.* [2014] using experimental data [*Coogan et al.*, 2014; *Wan et al.*, 2008]:

$$T(\mathrm{K}) = \frac{10000}{0.575 + 0.884\mathrm{Cr\#} - 0.897\ln(k_d)} \tag{1}$$

where

$$k_d = \frac{\mathrm{Al_2O_3^{olivine}}}{\mathrm{Al_2O_3^{spinel}}} \tag{2}$$

$$\mathrm{Cr\#} = \left(\frac{\mathrm{Cr}}{\mathrm{Cr+Al}}\right)^{\mathrm{spinel}} \tag{3}$$

Uncertainties in each parameter are reported by *Coogan et al.* [2014], though we use an estimate of total uncertainty in temperature, as described in section 4.2.

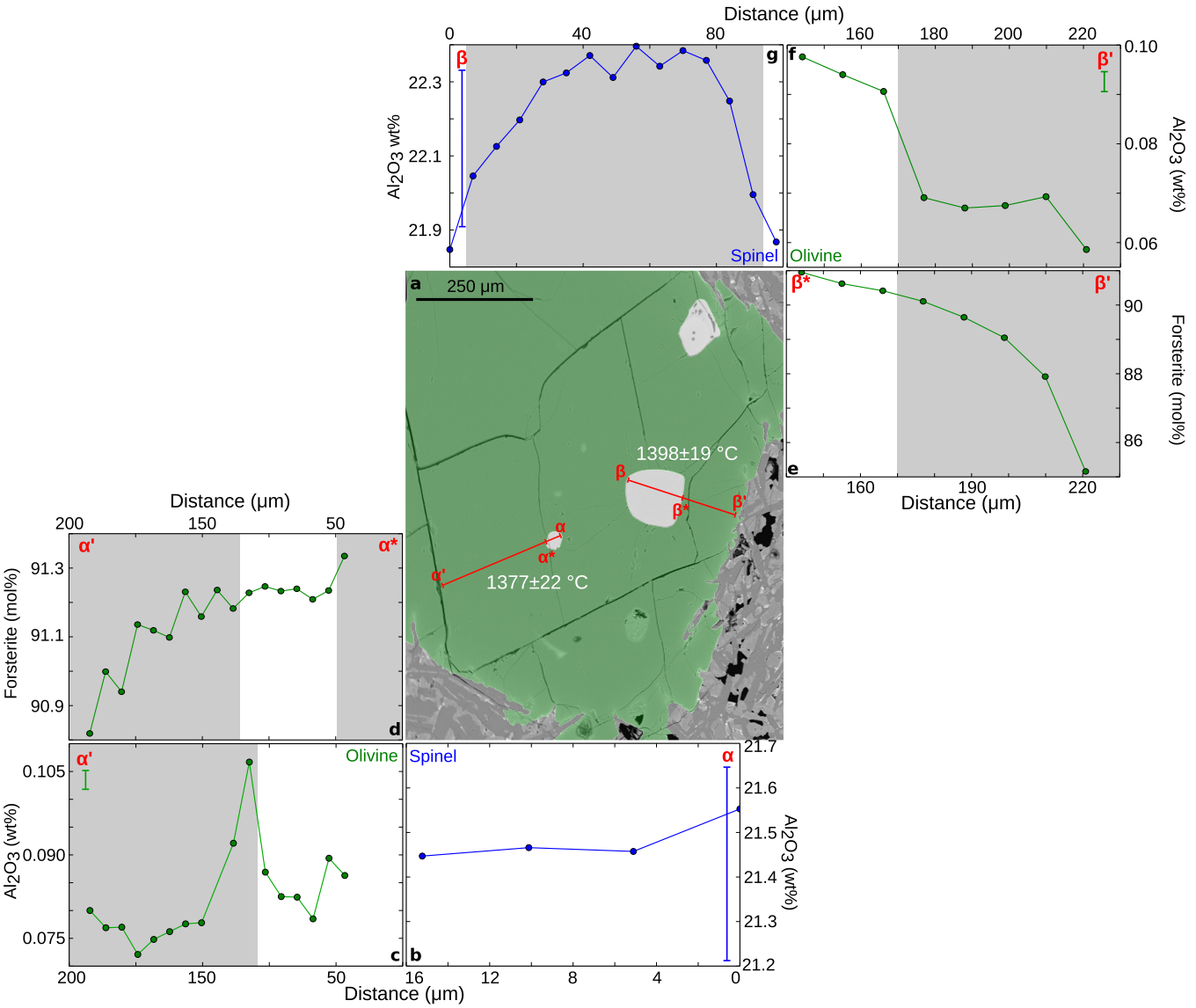

Figure 3. (a) Backscatter Electron Image and chemical data for Borgarhraun olivine crystal BH47-1. The olivine macrocryst has been colored green in the BSE image. Two profiles, (b–d) α–α^*–α' and (e–g) β–β^*–β', were measured by EPMA through both spinel and olivine as shown. The grey bars indicate points not included in the thermometry calculations. Representative one standard deviation analytical uncertainties are shown as green and blue bars. The temperature calculated for each profile and its uncertainty are shown on the BSE image.

4.1. Petrography and Chemistry of the Olivine and Spinel

Collection of profiles in spinel and olivine allowed the effect of both diffusion and growth zoning to be identified if present. Experimental studies suggest Al is a very slow-diffusing species in olivine [*Spandler and O'Neill*, 2009]; it is therefore likely that Al concentrations are primary and have not been reset. Sharp steps in Al concentration were observed along some olivine profiles, e.g., Figure 3f, most likely indicating multiple stages of crystal growth from magmas of different chemistry and temperature. Smooth variations in Al concentration and Cr# were seen in many of the profiles through the spinel inclusions, rising to a maximum in the center in some cases, e.g., Figure 3g, and a minimum in others. If postentrapment Al exchange between spinel and olivine was responsible for the zoning, very large changes in Al concentration in the olivine would be required in order to satisfy mass balance. No corresponding gradients in Al concentration were observed in adjacent olivine indicating that the spinel zoning does not arise from Al exchange with the olivine, and therefore formed prior to the spinel's trapping. The points at the spinel rims in contact with olivine are therefore the most likely to have been in Al equilibrium with the olivine that crystallized at the time of spinel trapping. We therefore use these measurements in our calculations.

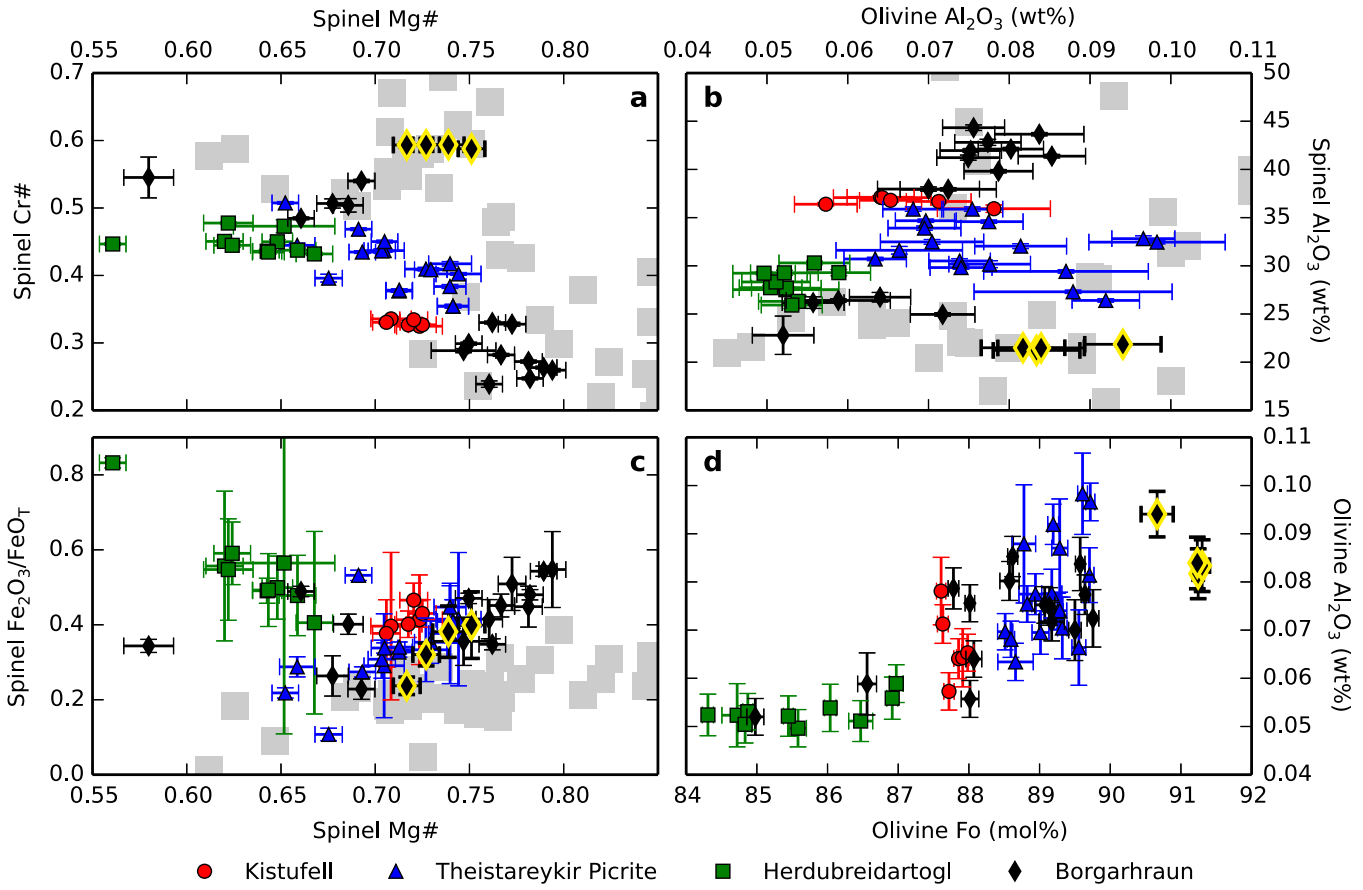

Figure 4. Olivine and spinel chemistry for the crystals used in this study. The grey squares are experimental data from *Wan et al.* [2008] and *Coogan et al.* [2014] used to calibrate the thermometer by *Coogan et al.* [2014]. (a, c) Spinel Mg# is calculated using FeO derived from a charge balance calculation. Error bars indicate analytical precision and natural variability in the crystal. The Borgarhraun points with a yellow outline are the four high-temperature points used in the calculation of mantle temperature.

Coogan et al. [2014] emphasize the importance of phosphorus in enhancing the uptake of Al in olivine, and recommend extrapolating Al_2O_3 concentration back to 0 wt % P_2O_5. The phosphorus concentration in all crystals analyzed in this study was low (typically less than 100 ppm P_2O_5) and showed no correlation with Al in the vast majority of crystals. Where there was a correlation, the average Al_2O_3 of the low-phosphorus points was within one standard deviation of the value obtained by a linear regression back to 0 wt % P_2O_5.

Figure 4 shows that the majority of the crystals, particularly those recording the highest temperatures, are well within the bounds of the crystal compositions used in the experimental calibration of the thermometer. This includes the Mg# and Cr# of the spinel, olivine and spinel Al concentrations, and the estimated Fe_2O_3/FeO_T ratio calculated by charge balance. The Mg# is defined as

$$\mathrm{Mg\#} = \frac{\mathrm{Mg}}{\mathrm{Mg} + \mathrm{Fe}^{2+}} \tag{4}$$

where each quantity is in moles. The spinel crystals that have higher Fe_2O_3/FeO_T ratios than the calibration have the lowest crystallization temperatures. Since the lowest crystallization temperatures are not used in the T_p inversion (justified in section 4.3), these high Fe_2O_3/FeO_T ratios have no further consequence in this study.

4.2. Error Propagation

For each olivine-spinel pair, the olivine-spinel Al-exchange temperature and its uncertainty were calculated by applying a Monte Carlo error propagation. Values for each chemical parameter used in the thermometer (olivine and spinel Al_2O_3, and spinel Cr#) were selected at random from Gaussian distributions defined by the mean and standard deviation of the measurement. The analytical precision for Al_2O_3 was $1\sigma = 38$ ppm

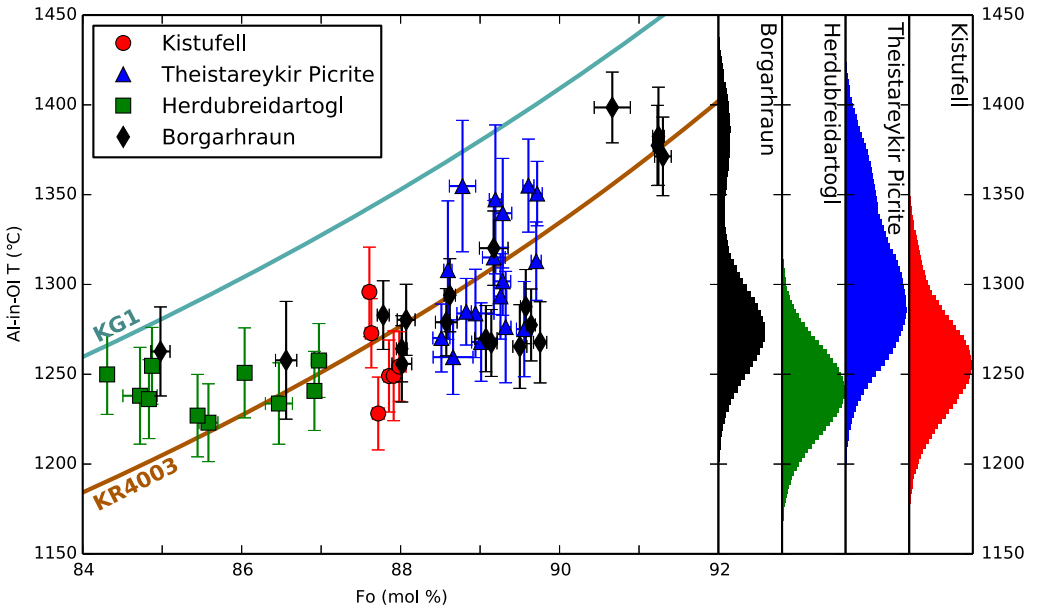

Figure 5. Olivine-spinel aluminum exchange temperatures for our Iceland data set. The distributions on the right show the summed Monte Carlo distributions for each eruption. The two lines show the evolution of olivine fractionation, calculated using Petrolog3 [*Danyushevsky and Plechov*, 2011] and the *Beattie* [1993] olivine partitioning model at 0.8 GPa, QFM. The starting compositions used were experimental liquids derived from KR4003 at 3.0 GPa, 1540°C [*Walter*, 1998], and KG1 at 3.0 GPa, 1525°C [*Kogiso et al*., 1998] (the two end-member melts identified as best describing primitive NVZ melts by *Shorttle and Maclennan* [2011]).

in olivine, and $1\sigma = 0.17$ wt % in spinel, though a (1σ) relative error of 2.0% based on EPMA counting statistics was used instead for Al_2O_3 in spinel. For spinel Cr#, the precision was $1\sigma = 0.0020$. Repeat analyses of olivine and spinel crystals were paired at random. The temperature calculated from the randomly picked chemical parameters was then used as the mean for the definition of a Gaussian distribution representing the calibration uncertainty. The standard deviation for the uncertainty in the thermometer calibration was taken to be 14°C, obtained from the distribution of data around the empirical regression through the experimental data. This process was repeated 10,000 times for each olivine-spinel pair in order to obtain a distribution, from which a mean and standard deviation could be calculated. The propagated uncertainty in temperature estimate is typically ~20°C and is similar in magnitude to that reported by *Spice et al*. [2016] and *Wan et al*. [2008]. Some crystals have a greater uncertainty, arising from their internal heterogeneity and the associated uncertainty in how to pair olivine and spinel analyses. Where single olivine crystals had multiple spinel inclusions, analyses pairing each spinel inclusion with the adjacent olivine gave temperature estimates within their mutual uncertainty.

4.3. Thermometry Results

Crystallization temperature estimates for the Northern Volcanic Zone (NVZ) are shown in Figure 5. The histograms in Figure 5 show offsets and variable widths in crystallization temperature distributions between each eruption. The scatterplot shows that the variation in crystallization temperature between eruptions covaries with their olivine forsterite content. Since the forsterite content of crystallizing olivine decreases during fractional crystallization, it can be used as a proxy for melt evolution. The evolution of temperature during fractionation is shown in Figure 5 by solid blue and red lines, for KG1 and KR4003-derived melts, respectively [*Kogiso et al*., 1998; *Walter*, 1998]. The caption to Figure 5 describes this crystallization calculation. These melts represent the end-member melt compositions entering the Icelandic NVZ crust [*Shorttle et al*., 2014]. Much of the range in crystallization temperature can be accounted for by the cooling associated with fractional crystallization, and the deviations from this are consistent with the range of crystallization temperatures that would arise from melts with variable composition (and therefore liquidus temperature) arriving from the mantle. Crystallization temperatures recorded in the Borgarhraun crystals extend over much of the range of the data set, and therefore the data set does not resolve differences in mantle temperature within Iceland. The difference in position and shape of the histograms represents biased sampling of the history of fractional crystallization by each eruption.

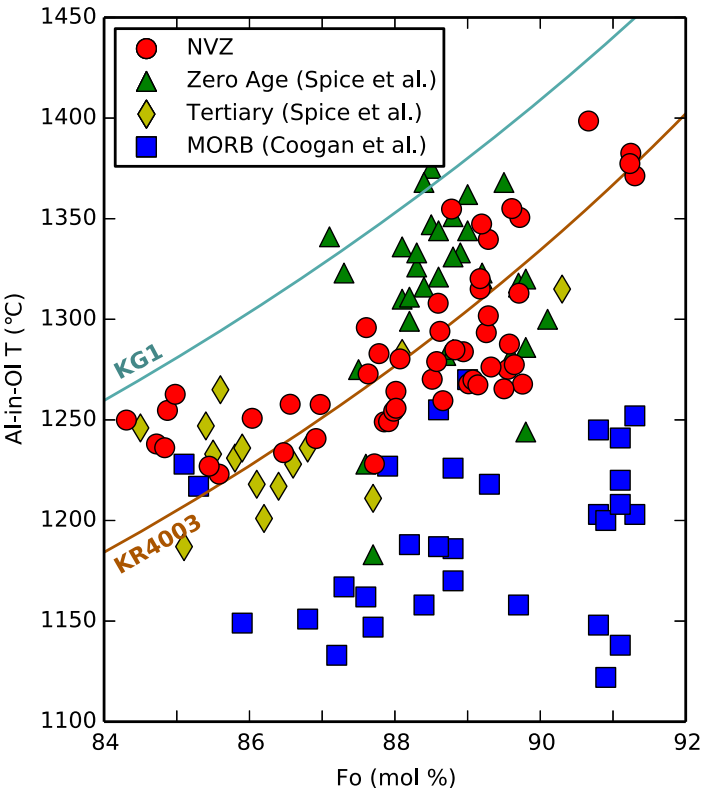

Figure 6. Comparison of our olivine-spinel aluminum exchange temperatures for Iceland's NVZ with the olivine-spinel aluminum exchange temperatures for zero-age and Tertiary Iceland from *Spice et al.* [2016], and the data set for MORB from *Coogan et al.* [2014]. Uncertainty for our data set is shown in Figure 5 but is of a similar magnitude to the ±22°C uncertainty of the *Spice et al.* [2016] and *Coogan et al.* [2014] data sets. Lines show fractional crystallization models as described in the caption to Figure 5.

4.4. Comparisons With Published Data and Relationship to Mantle Temperature

Figure 6 shows the same data compared with the crystallization temperatures reported for Iceland by *Spice et al.* [2016] and those for MORB by *Coogan et al.* [2014]. The *Spice et al.* [2016] zero-age crystallization temperatures are consistent with the range found in our data set. The range of temperatures at a given olivine composition in Figure 6 hints at spatial and temporal variability in the parameters controlling crystallization temperature. The highest temperatures in the combined data set are for Fo $_{>90}$ Borgarhraun crystals from this study, though there are no olivine crystals with a similar composition in the *Spice et al.* [2016] data set. In addition to zero-age eruptions, *Spice et al.* [2016] reported results from Tertiary flows, arguing that their offset in crystallization temperature is consistent with a cooler mantle in the Tertiary, as indicated by other mantle temperature proxies. However, taking into account olivine forsterite content, the crystallization temperatures for Tertiary Iceland overlie the range of temperatures reported from young Icelandic olivines in this paper. The temperature offset observed by *Spice et al.* [2016] could therefore be consistent with an undersampling of primitive, higher temperature olivine crystals in the Tertiary eruptions they studied, rather than being a signal of lower plume temperatures in the Tertiary. In contrast, a consistent offset to lower crystallization temperatures is seen in the MORB data set relative to Iceland at all olivine forsterite contents. In order to generate such an offset, the melt compositions, in particular the MgO and FeO concentrations, supplied from the mantle must be different. In section 5, we consider the role of both lithology and temperature in accounting for this observation.

Using offsets in crystallization temperature distribution as a proxy for mantle temperature, without controlling for differences in extent of fractional crystallization, would lead to inferring mantle T_p both increases and decreases with distance along the NVZ away from the plume center. By examining the relationship between crystallization temperature and melt evolution, for which we use olivine forsterite content as a proxy (Figure 5), it is clear that the offset in position of the histograms shown on the right of Figure 5 are not controlled by variations in mantle temperature. A more robust observation to link to mantle T_p is the crystallization temperature of primitive melts. Olivine crystals from Borgarhraun of Fo_{91} are assumed to be in equilibrium with mantle olivine and therefore the first crystals to have grown from mantle-derived melts. When inverting for mantle T_p (section 5.5), we use the crystallization temperatures of the most forsteritic crystals. For Iceland these forsteritic crystals are from Borgarhraun, for the MORB data set of *Coogan et al.* [2014], the most forsteritic crystals are from the Siqueiros Fracture Zone.

5. Thermal Model

Since the highest crystallization temperatures are observed in the most forsteritic olivine crystals, they likely reflect crystallization of melts derived directly from the mantle. As discussed in section 1, the diversity in

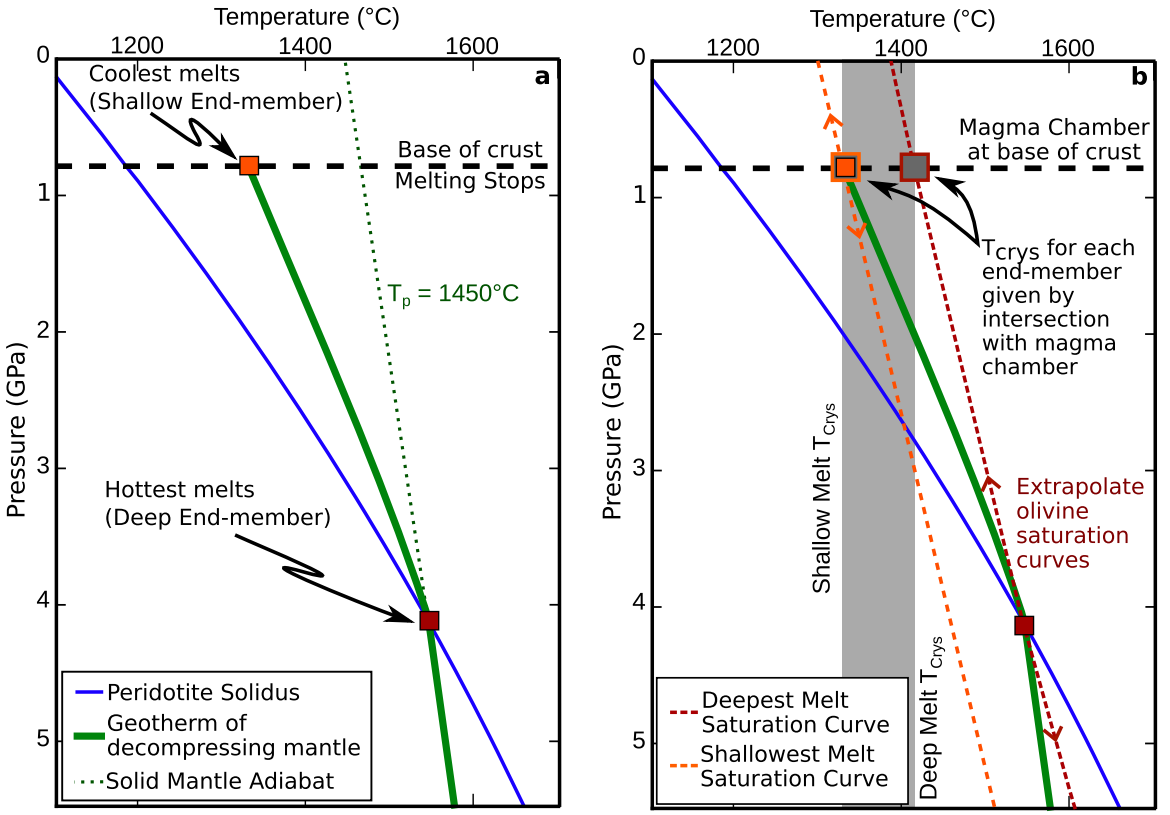

Figure 7. Schematic illustration of our thermal model in the simplest case of melting a 100% lherzolite mantle with T_p = 1450°C. (a) How the end-member melts are selected, after calculating the geotherm. (b) How olivine saturation curves are extrapolated from each of the points selected in Figure 7a. Finding the intersection of these curves with the base of the crust (assumed to be where crystallization begins) allows estimation of the olivine saturation temperature of both end-member melts.

melt inclusion chemistry seen in such crystals indicates fractional mantle melts are not completely homogenized before leaving the mantle. These fractional melts are derived at different pressure and temperature conditions, therefore their major element chemistry, including MgO and FeO concentrations, will also be diverse. Since the temperature of olivine saturation is a function of both MgO and FeO concentration [*Roeder and Emslie*, 1970], different melts derived from mantle of the same T_p will reach olivine saturation at different temperatures. We present a forward model to understand the uncertainty this process introduces into converting crystallization temperatures into mantle T_p.

Olivine saturation is modeled here; however, it is the cosaturation temperature of olivine and spinel that is recorded by the Al-exchange thermometer. Though experimental data suggests spinel may saturate before olivine [*Maaløe and Jakobsson*, 1980], the presence of spinel inclusions in the most forsteritic olivine crystals suggests spinel saturated before or very soon after olivine saturation. Therefore, it is very unlikely that the requirement for both olivine and spinel saturation in the melt requires a significant cooling (or differentiation) interval.

There are a number of steps in the process used to extract mantle temperature estimates, which are summarized sequentially:

1. A multicomponent melting model (described comprehensively by *Shorttle et al.* [2014], and more generally by *Phipps Morgan* [2001]) is used to calculate the thermal structure and melt fraction for many individual melting regions with variable mantle temperature (T_p) and differing proportions of pyroxenite and harzburgite (ϕ_{Px}, ϕ_{Hz}) (section 5.2 and Figures 7a, 8a, and 8b).
2. Crustal thickness (t_c) is calculated from the melt fraction against depth curve, assuming mid-ocean ridge corner flow. We stop melting in the model once mantle upwells to the base of the crust.
3. The fraction of bulk crust (i.e., the fully mixed melt) derived from pyroxenite is calculated (F_{Px}).

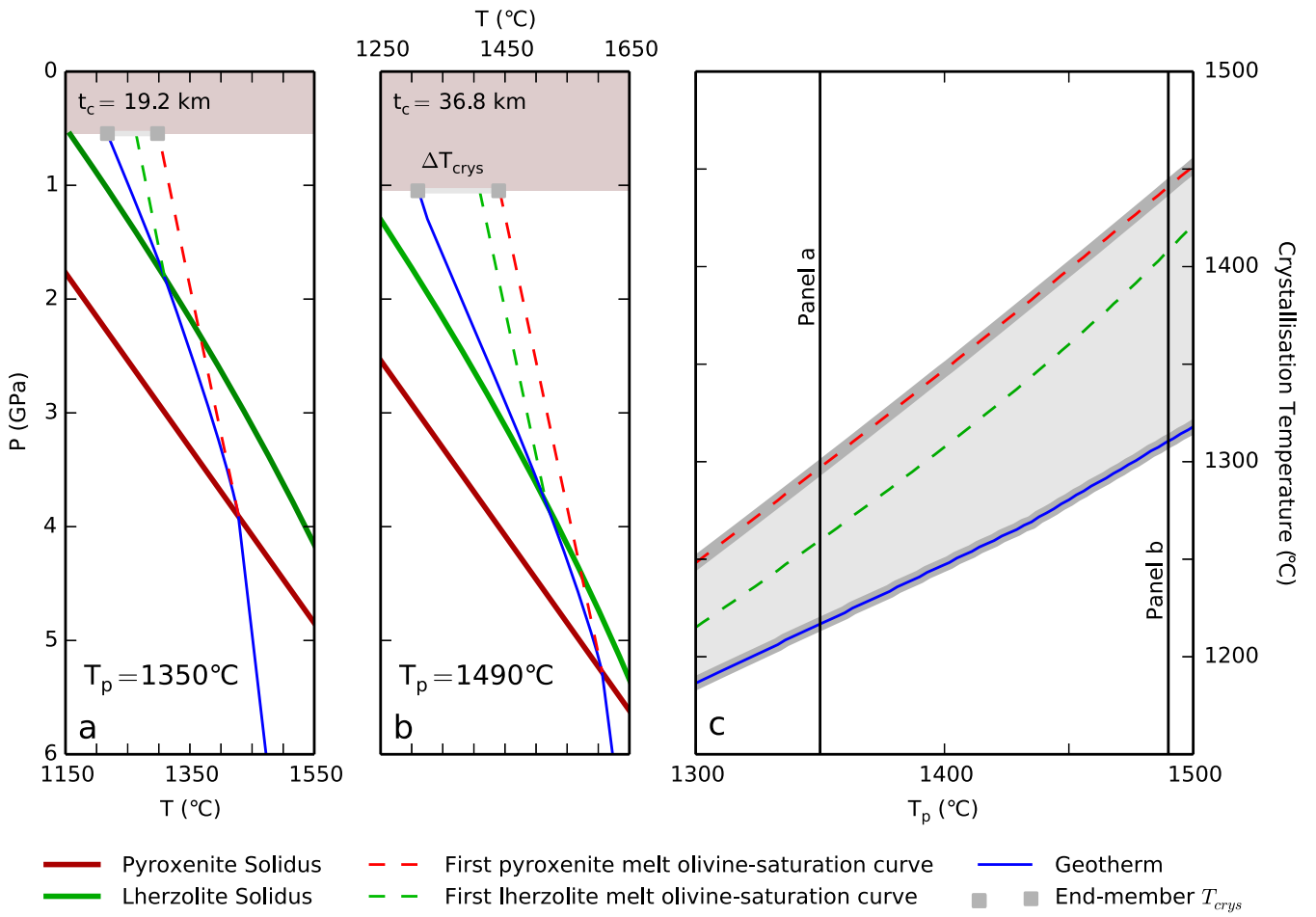

Figure 8. (a, b) The geotherms (blue) for adiabatically ascending mantle of 70% lherzolite and 30% pyroxenite undergoing melting for T_p = 1350°C and T_p = 1490°C, respectively. The olivine-saturation curves for two deep melts (first pyroxenite and lherzolite melts) are shown by the dashed lines. The olivine saturation curves are omitted for the shallow melt bound since the olivine saturation temperature at the base of the crust coincides with the geotherm. The produced crustal thickness (t_c) is shown by the filled box. The range of olivine saturation temperatures of primitive melts generated by each model is shown by the small-grey, light-grey boxes. (c) The range of olivine saturation temperatures of primitive melts for the same mantle composition as a function of T_p.

4. Hypothetical end-member melts from the base and top of the melting region, representing absolute limits of fractional melt diversity, are considered from each melting region modeled (Figure 7a). The temperature at which each end-member melt is saturated in olivine at the base of the crust is estimated (T_{crys}), since we assume this is where the magma chamber resides (section 5.1 and Figure 7b).
5. This set of modeled melting regions constitutes the forward model. When the results are plotted for fixed mantle T_p (Figure 9), two surfaces bound possible crystallization temperatures of primary melts arriving from the mantle. One surface represents fractional melts with a deep origin; the other represents shallow fractional melts. Variable mixing of melts derived between these two end-members (or reequilibration with the mantle) will result in an intermediate crystallization temperature.
6. By finding the melting region which simultaneously satisfies t_c, F_{Px}, and T_{crys}, the forward model is inverted to obtain T_p, ϕ_{Px}, and ϕ_{Hz}. Since each melting region model has two end-member T_{crys} bounds, there are two solutions: one assuming the observed T_{crys} arose from a deep-originating fractional melt, and one assuming a shallow origin. The T_p inferred differs for each solution due to the different magnitude of temperature correction required. A shallow melt has experienced significant cooling due to the latent heat of fusion, thus requiring a large temperature correction. A deep melt has experienced no such cooling, is intrinsically warmer and thus requires no temperature correction for melting, though will saturate in olivine at a slightly lower temperature than its melting temperature in a magma chamber at the base of the crust (due to the pressure dependence of saturation temperature).

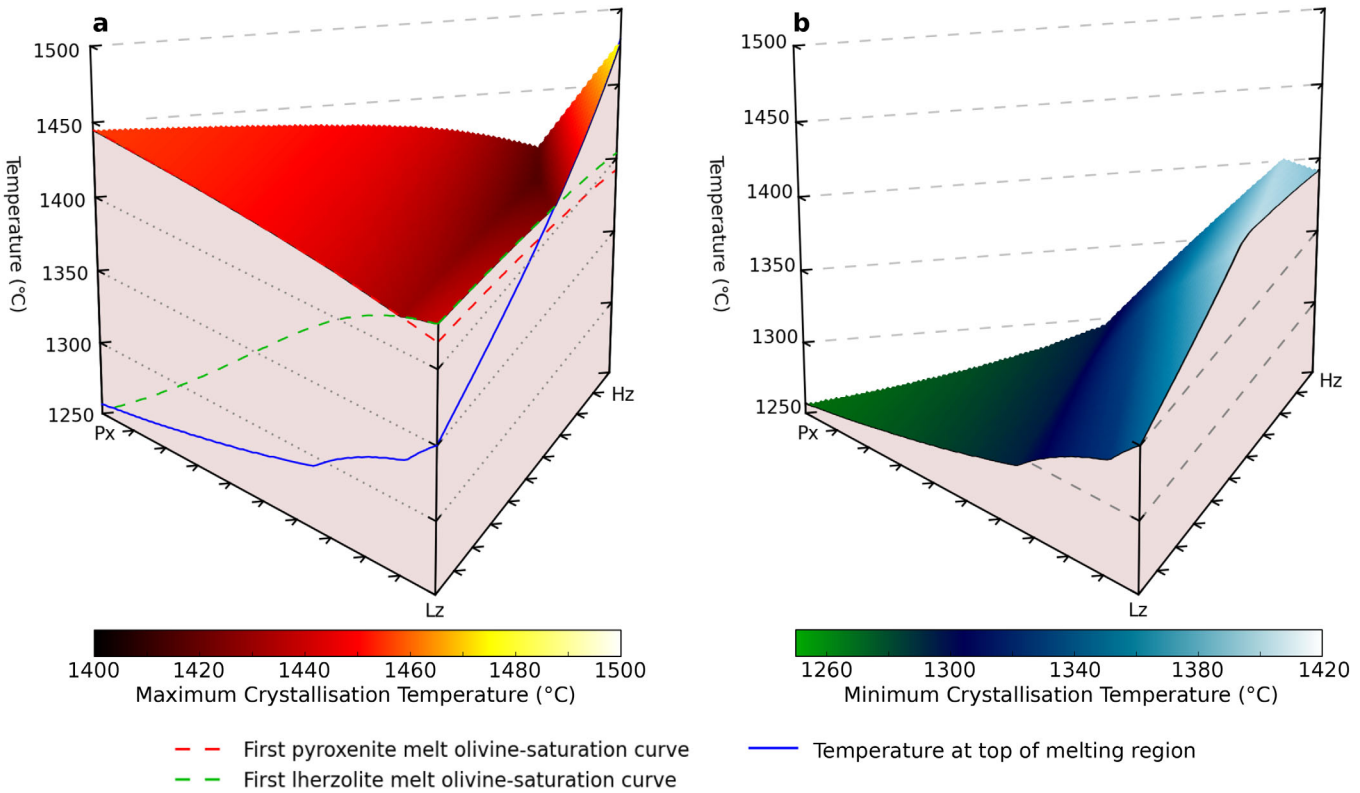

Figure 9. Crystallization temperatures of primary melts derived from a $T_p = 1480$°C mantle, as a function of lithology. (a) The surface of maximum crystallization temperature, and the lines show the crystallization temperatures of end-member melts for the lherzolite-pyroxenite and lherzolite-harzburgite joins. (b) The minimum crystallization temperature, which is identical to the temperature of the geotherm at the top of the melting region (except at high ϕ_{Hz}), since olivine crystallization is defined at the same depth.

7. This process is repeated 10^6 times for different values of t_c, F_{Px}, and T_{crys}, as defined by their uncertainties, in a Monte Carlo error propagation.

This is analogous to the method used by *Putirka* [2005], *Putirka et al*. [2007], and *Putirka* [2008a, 2016] in that estimated melt fraction determines the magnitude of the latent heat of fusion correction. We obtain the magnitude of the correction by finding the best-fitting geotherm (as illustrated in Figures A1 and A3). The steps in this process are discussed in detail below.

5.1. Effects of Melting and Melt Transport on Olivine Saturation Temperature

Mantle of a single T_p will melt over a range of temperature as the mantle is cooled by latent heat of fusion and adiabatic expansion. The highest melting temperatures will occur at the onset of melting, and the lowest at the top of the melting column where the mantle has undergone the most melt extraction, as shown in Figure 7a. Without reconstructing the chemistry of the magmas parental to the olivine and spinel crystals, the depth at which they were generated, and therefore the magnitude of the correction required for the latent heat of melting, is uncertain. We therefore consider two end-member cases: melts formed at the base of the melting region, and those formed at the top of the melting region.

Once a melt has been generated it ascends through the mantle by diffuse or channelized flow, at a greater speed than the solid matrix [*McKenzie*, 1984; *Spiegelman and Kelemen*, 2003]. As soon as the magma leaves its source, it will be out of thermal and chemical equilibrium. The magma is in chemical disequilibrium because the equilibrium magma composition depends on temperature, pressure, and matrix composition, all of which have changed. Higher up in the melting region, more sensible heat has been converted to the latent heat of fusion, and the matrix will thus be cooler than the melts generated beneath it. The extent to which equilibrium can be reestablished depends upon the timescale of heat diffusion (for thermal equilibrium) and mass transfer (for chemical disequilibrium). If, by thermally reequilibrating, the magma becomes oversaturated or undersaturated in olivine, additional chemical disequilibrium is generated. In order for

olivine saturation to be reestablished, the melt must gain or lose MgO and FeO by precipitating or dissolving olivine. The melt may also be out of chemical equilibrium if its Mg# is not in equilibrium with the Mg# of the matrix. Since the Mg# does not uniquely determine the temperature at which olivine is saturated in the melt [*Roeder and Emslie*, 1970], this component of chemical equilibrium is not considered further here.

The MgO and FeO contents of magmas derived from an upwelling column of mantle vary with depth, therefore the temperature at which the magma will saturate in olivine in a magma chamber at the base of the crust must also vary. *Putirka* [2008b], after *Helz and Thornber* [1987], parametrized the temperature of olivine saturation with pressure and melt composition. The relationship between olivine saturation temperature and pressure can be described by the olivine saturation curve, equivalent to the liquidus of a magma when olivine is the first phase to saturate. Since the temperature of olivine saturation depends on magma composition, different fractional melts will have their own olivine saturation curve. The composition of the magma parental to the olivine crystals is unknown, but since the magma is saturated in olivine when it forms, one point of the olivine saturation curve must be the pressure and temperature of magma formation. By making the curve intersect the pressure and temperature of magma formation, the compositional dependence of the olivine saturation curve is accounted for. The remaining term is the pressure dependence, which can be used to extrapolate the curve to low pressure. This process is shown schematically by the dashed lines in Figure 7b. If melts arrive at a higher temperature than the saturation temperature (and have not reequilibrated by dissolving olivine from the matrix) they may need to undergo cooling before olivine saturation. If melts arrive at a lower temperature than their predicted saturation temperature, either the MgO and FeO concentrations will have reequilibrated at this temperature by precipitating olivine, or they will be supercooled and the first olivine to crystallize will do so at the melt's arrival temperature. Since the shallow melt end-member (Figure 7b) represents melt derived at the temperature of the matrix at the top of the melting region, melts cannot become supercooled below this temperature during transport. The two end-member bounds therefore define the range of possible olivine saturation temperatures; any reequilibration during transport will shift the saturation temperature between these bounds.

If some amount of disequilibrium prevails during melt transport it is possible for the same olivine saturation temperature to be produced by mantle regions of different T_p. The partial reequilibration process therefore introduces uncertainty in relating crystallization temperature to mantle potential temperature. Although it is likely that the magmas will undergo some amount of reequilibration during their ascent, this cannot be quantified without making further assumptions. By taking the saturation temperatures of the deepest and shallowest melts (assuming complete disequilibrium) as bounds, the uncertainty introduced by partial reequilibration during transport can be included in the T_p estimates. The shallowest melt production, and therefore the top of the melting region, is assumed to coincide with the base of the crust, calculated from the melting model using *White et al*. [1992, equation (6)].

When modeling olivine saturation temperatures, an estimate of the crystallization pressure is required. Pressure estimates for crystallization derived from clinopyroxene-melt equilibria in Borgarhraun lava flows by *Winpenny and Maclennan* [2011] indicate crystallization of primitive melts takes place at a mean pressure of 8.1 kbar, near or below the Moho. In the models presented here, the magma chamber is placed at the base of the crust, as calculated from the melting model. In consequence, the olivine saturation temperature for the shallow melt end-member is equal to the matrix temperature at the top of the melting region.

5.2. Effects of Lithological Heterogeneity on the Thermal Structure of the Melting Region

The diversity in Pb-isotope ratios observed in melt inclusions from single Icelandic eruptions [*Maclennan*, 2008] indicates that the Icelandic mantle hosts high-amplitude chemical variability within single melting regions. This isotopic heterogeneity is likely to map onto lithological heterogeneity in the Icelandic mantle [*Chauvel and Hémond*, 2000; *Shorttle and Maclennan*, 2011].

The presence of pyroxenitic components in the Icelandic mantle has been inferred using a variety of trace element, isotop, and major element tracers [*Chauvel and Hémond*, 2000; *Stracke et al*., 2003a; *Kokfelt et al*., 2006; *Sobolev et al*., 2008; *Shorttle and Maclennan*, 2011]. In contrast, *Herzberg et al*. [2016] argue for a pyroxenite-free mantle below Iceland on the basis of low olivine Ni concentrations from three eruptions in Theistareykir. However, the discrepancy between *Shorttle et al*. [2014] and *Herzberg et al*. [2016] can be reconciled by the fact that chemically variable melts are supplied to the crust, representing different contributions from pyroxenitic and lherzolitic lithologies. The three eruptions studied in *Herzberg et al*. [2016] are all

depleted (Nb/Zr $\leq$ 0.06) and are in the population identified by *Shorttle et al*. [2014]; *Shorttle and Maclennan* [2011] as representing partial melts of lherzolite. These samples therefore do not represent the enriched components present in other Icelandic neovolcanic zone eruptions, such as Gaesafjöll and Stapafell, the major element and olivine minor element chemistry of which *Shorttle and Maclennan* [2011] showed to be consistent with partial melting of a KG1-like lithology. Although the highest crystallization temperatures we observe are from a geochemically depleted eruption in Theistareykir, and therefore have little contribution from a pyroxenite source, pyroxenite must still be considered as its presence in the melting region will influence the thermal structure of the melting region.

Shorttle et al. [2014] additionally argue the Iceland plume must contain a significant quantity of harzburgite in order to reconcile the volume and the chemistry of Icelandic volcanism with estimates of the plume volume flux [*Jones et al*., 2014]. While *Brown and Lesher* [2014] show that crustal thickness and Nd-isotope observations, from both central and coastal Iceland, can be reconciled with a lherzolite-pyroxenite mantle, they do not consider the additional constraint of matching plume volume flux [*Jones et al*., 2014] and therefore do not find a requirement for harzburgite components as *Shorttle et al*. [2014] do. As we discuss in section 5.3, we do not consider plume buoyancy or volume flux here but do allow the fraction of harzburgite to vary from 0% in our models.

Lithological heterogeneity exerts a control on both magma chemistry and the thermal evolution of the mantle during decompression melting [*Sleep*, 1984; *Phipps Morgan*, 2001; *Stolper and Asimow*, 2007]. To incorporate the effect that lithological heterogeneity will have on possible crystallization temperatures, we model the end-member scenario of a mechanical mixture of fusible and refractory components within lherzolite, using the model described by *Shorttle et al*. [2014]. We use the *Katz et al*. [2003] parameterization of KLB-1-like lherzolite melting, the *Pertermann and Hirschmann* [2003] G2 pyroxenite parameterization for pyroxenite melting, and assume harzburgite does not melt, following *Shorttle et al*. [2014]. A comprehensive description of the melting model is given by *Phipps Morgan* [2001] and *Shorttle et al*. [2014]. In Appendix B, we discuss using a KG1 pyroxenite parametrization [*Shorttle et al*., 2014] in place of the G2 pyroxenite. Complete thermal equilibrium between the solid components is assumed. Since the thermodynamic properties of each of the sources are poorly constrained, we set them all to the values given in *Katz et al*. [2003].

5.3. Effects of Mantle Flow Field on the Melting Region

In order to account for the thickness (38–40 km) [*Darbyshire et al*., 1998] and composition of the crust in central Iceland, a mantle flow field with a substantial component of plume-driven upwelling is required. However, the thickness (20–21 km) [*Darbyshire et al*., 2000] and composition of the crust at Theistareykir, near the northern coast of Iceland, are consistent with passive plate-driven upwelling [*Maclennan et al*., 2001]. Since our crystallization temperature data set shows no significant temperature offset with along-axis distance, and our highest temperature crystals are from the northern part of the Northern Volcanic Zone, we do not consider the effects of plume-driven upwelling further.

5.4. Forward Model of Mantle Melting

The behavior of the model for mantle containing lherzolite and pyroxenite in mass proportions of ϕ_{Lz}=70% and ϕ_{Px}=30% is illustrated in Figure 8. End-member melts generated at the point of initial solidus intersection for each lithology, and at the top of the melting region are considered. Increasing the mantle potential temperature causes the olivine saturation temperature of each end-member melt to rise, since both melts are then generated at higher temperatures. Olivine saturation temperatures at the base of the crust are calculated using the olivine saturation curves described in section 5.1. For each T_p, a range of crystallization temperatures is calculated, corresponding to the diversity of fractional melts generated. Increasing the mantle potential temperature also increases the range of olivine saturation temperatures of primary melts. The deepest melts are produced deeper and at a higher temperature, and more cooling occurs due to the longer melting interval, thereby reducing the temperature of the shallowest melts. In a ϕ_{Lz}=70% and ϕ_{Px}=30 % mantle, a T_{crys} = 1300°C crystallization temperature would be consistent with a mantle T_p of 1350–1470°C. The low T_p bound assumes the melt parental to the crystals is derived from the base of the melting region, and therefore requires zero latent heat of fusion correction. The high T_p bound assumes derivation of the melt from the top of the melting region, requiring the maximum latent heat of fusion correction.

The effect of varying mantle lithology proportions, while maintaining a fixed T_p, is shown in Figure 9. As ϕ_{Px} rises, the range in T_{crys} increases dramatically. The decrease in temperature of the lower T_{crys} surface (blue-green in Figure 9) arises from the greater productivity of pyroxenite relative to lherzolite resulting in a greater total melt fraction and therefore more sensible heat consumption during melting. The increase in T_{crys} of the upper surface (red-yellow in Figure 9) originates from melts pooling at the base of a thicker crust; the temperature of melt formation is unchanged since it is controlled by the pyroxenite solidus. Since the olivine saturation curve has a positive gradient in pressure-temperature space, a melt of a given composition will saturate in olivine at a higher temperature at greater pressure.

As harzburgite fraction ϕ_{Hz} increases, Figure 9 shows an initial contraction, followed by expansion, of T_{crys} range. Increasing ϕ_{Hz} causes the proportion of melting lithologies to decrease: less melt is produced and less thermal energy consumed. Melts are therefore produced over a narrower temperature range. Where the temperature at the top of the melting region becomes greater than the temperature of olivine saturation in deeply derived melts at high ϕ_{Hz} in Figure 9, the range in T_{crys} begins increasing again. When ϕ_{Hz} is sufficiently high, the geotherm (blue line in Figure 9) becomes very close to the solid adiabat (green dashed line in Figure 7). Since the olivine saturation curve has a shallower gradient than the solid adiabat in pressure-temperature space (Figure 7), shallower melts will now crystallize at higher temperatures than deep melts. The inversion results discussed in section 5.5 do not result in high ϕ_{Hz} solutions, it is therefore valid to equate the two surfaces with shallow and deep melts in the context of these results. A similar effect is seen for small values of ϕ_{Px}. In the pyroxenite-only melting region, the geotherm may remain very close to the solid adiabat until lherzolite melting begins. This is shown by the crossing green and red dashed lines on Figure 9a.

5.5. Inverting for T_p

The forward model (section 5.4) shows that varying mantle lithology can cause crystallization of primitive mantle melts over a temperature range of over 200°C, even at constant mantle T_p. Differences in crystallization temperatures of primary melts between two locations could therefore be explained by a variable mantle lithology or processes of melt extraction (i.e., how biased toward deep or shallow melt production the crystallization temperatures are), rather than by T_p variations.

The simplest case is to assume a lherzolitic (ϕ_{Lz}=100%) mantle. The Fo_{91} crystals from Iceland (outlined in yellow in Figure 4) have a mean T_{crys} of 1385°C, which the inverse model shows is consistent with a T_p of 1430–1520°C (lower left corner of Figure 10). For the Siqueiros Fracture Zone (MORB), the four highest T_{crys} points in the *Coogan et al.* [2014] data set have a mean of 1253°C, which the inverse model shows is

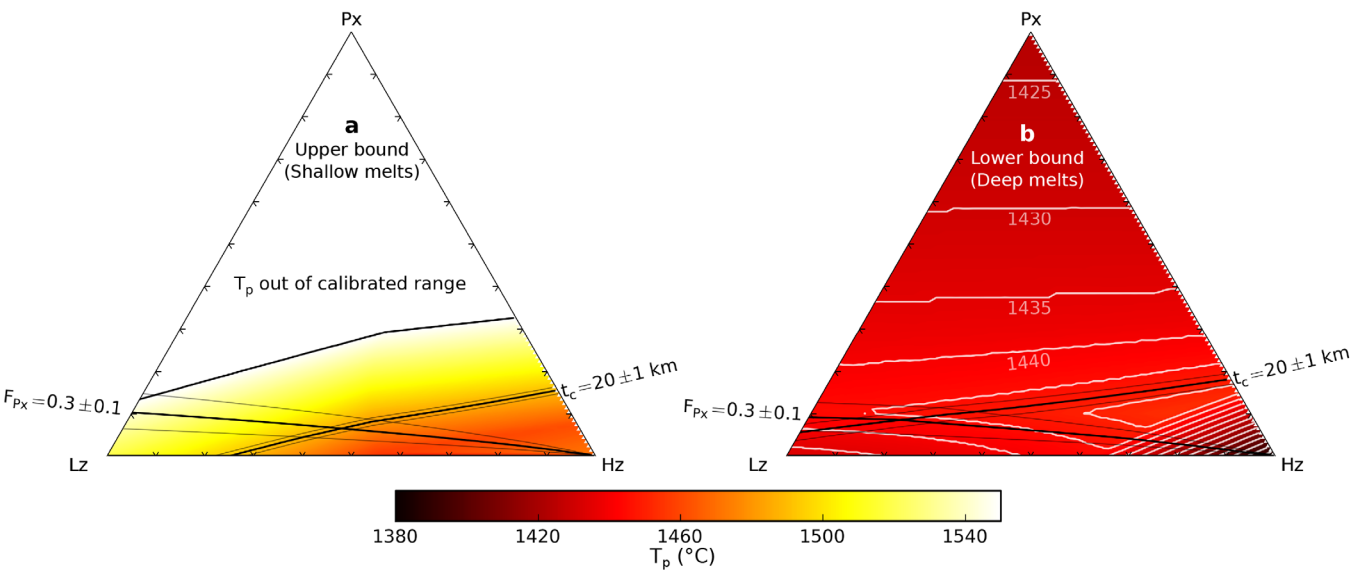

Figure 10. (a) Upper and (b) lower bounds on mantle T_p as a function of mantle lithology, inferred from a crystallization temperature of 1385°C. (a) The upper bound corresponds to shallow melts and (b) the lower bound to deep melts, apart from at high ϕ_{Hz} as shown in Figure 9. White contours are T_p in °C. Also shown are lines for t_c=20±1 km and F_{Px}=0.3±0.1. At the highest T_p, the melting pressure and temperature are far beyond the conditions at which the melting model is calibrated.

Table 1. Input Parameters and Their Source for the Iceland and Siqueiros Model Inversions[a]

Parameter	Value	Source
Iceland		
t_c	20 ± 1 km	*Darbyshire et al.* [2000]
F_{Px}	0.3 ± 0.1	*Shorttle et al.* [2014]
T_{crys}	1385°C[b]	This study
Siqueiros		
t_c	5.74 ± 0.27 km	*Aghaei et al.* [2014]
F_{Px}	0.175 ± 0.1	*Hirschmann and Stolper* [1996]
T_{crys}	1253 ± 25°C	*Coogan et al.* [2014]

[a]Uncertainties are one standard deviation.
[b]Distribution of values from Monte Carlo thermometer error propagation, mean quoted here.

consistent with a T_p of 1270–1350°C. The range in consistent T_p arises from uncertainty in which fractional melt is parental to the high-T_{crys} olivine. Allowing the proportions of each lithology to vary between 0 and 100% results in the Iceland T_{crys} data being matched by a mantle T_p as low as 1385°C, if the mantle is harzburgitic, and in excess of 1550°C if the mantle is dominated by pyroxenite (Figure 10). The minimum bound (Figure 10b) on inferred mantle T_p shows very little variation with lithology, since as long as fusible pyroxenite is present this bound is controlled by the position of the pyroxenite solidus. The small variation in minimum inferred mantle T_p arises from the varying crustal thickness as the bulk mantle productivity changes, except at high ϕ_{Hz} where it instead corresponds to shallow melts as discussed in section 5.4 and Figure 9. The maximum bound on inferred mantle T_p is much more sensitive to lithology; since it corresponds to the shallowest melts (except at high ϕ_{Hz}) it is primarily controlled by the geothermal gradient in the melting region, which itself is strongly controlled by the bulk mantle productivity. Allowing lithology to vary for the inversion of the Siqueiros data shows T_{crys} can be matched by mantle T_p of 1253–1474°C. By varying mantle lithology, it is possible to match the observed variation in primary melt T_{crys} between Siqueiros and Iceland with the same mantle T_p.

The very lowest mantle T_p estimates arise from 100% harzburgitic mantle, i.e., mantle that has undergone no melting and so has followed the solid adiabat to the surface. This solution clearly does not match the 20 km crustal thickness observed at Iceland's coasts [*Darbyshire et al.*, 2000], or the substantial contribution of lherzolitic and pyroxenitic sources to the chemistry of erupted basalt [*Shorttle and Maclennan*, 2011]. Equally, the 100% pyroxenite mantle which results in the highest temperature estimates must produce 40–82 km thick crust to be consistent with the observed T_{crys}, and cannot explain the contribution of lherzolitic melts to basalt chemistry [*Shorttle and Maclennan*, 2011], nor be reconciled with plume buoyancy [*Shorttle et al.*, 2014]. There is in consequence a subset of solutions that are consistent with all observational constraints. Our inversion process uses three observations: crystallization temperature, T_{crys}, crustal thickness, t_c, and the proportion of bulk crust derived from pyroxenitic melts, F_{Px}, to invert for three variables in the model: mantle T_p, ϕ_{Px}, and ϕ_{Hz}, where $\phi_{Lz}=1-\phi_{Px}-\phi_{Hz}$.

The combination of the t_c and F_{Px} constraints with T_{crys} is illustrated in Figure 10; two points in lithology-T_p space, one for each of the low and high T_p bounds, can be identified that satisfy all three constraints. The values of the input parameters, and their sources, are given in Table 1. Since the highest crystallization temperatures and most forsteritic olivines in the *Coogan et al.* [2014] MORB data set are from the Siqueiros Fracture Zone, inversion parameters were chosen for Siqueiros, and are shown in Table 1. A Monte Carlo method (using 10^6 calculations) was used for the inversions, where values for F_{Px}, t_c, and, for Siqueiros, T_{crys} were selected with a probability defined by a Gaussian distribution. The mean Siqueiros T_{crys} value was taken as the mean of the four highest T_{crys} points. For Iceland, T_{crys} was selected at random from the distributions of T_{crys} estimates derived from the Monte Carlo error propagation of the thermometer; only the results from the four highest T_{crys} crystals were used. The input distributions are shown in Figures 11 (Iceland) and 12 (Siqueiros), plots d–f, as black lines.

5.6. Inversion Results

The results of the inversion for Iceland are shown in Figure 11 and for MORB in Figure 12. In each case, the results of the inversion (T_p, ϕ_{Px} and ϕ_{Hz}) are shown alongside the distributions of input parameters for which solutions were found. Medians and 95% confidence limits are given in Table 2. For each setting, two sets of solutions are found, one for the upper T_p bound arising from the cooler shallow melts (Figure 10a), and one for the lower T_p bound arising from the deeper hotter melts (Figure 10b).

For Iceland, solutions were found for all values of t_c and F_{Px} for both bounds, and for all T_{crys} values for the high T_p (shallow melts) bound. For the low T_p (deep melts) bound, no solutions were found for the lowest values of T_{crys}. As T_{crys} decreases the solution T_p must decrease and ϕ_{Px} must increase in order to match

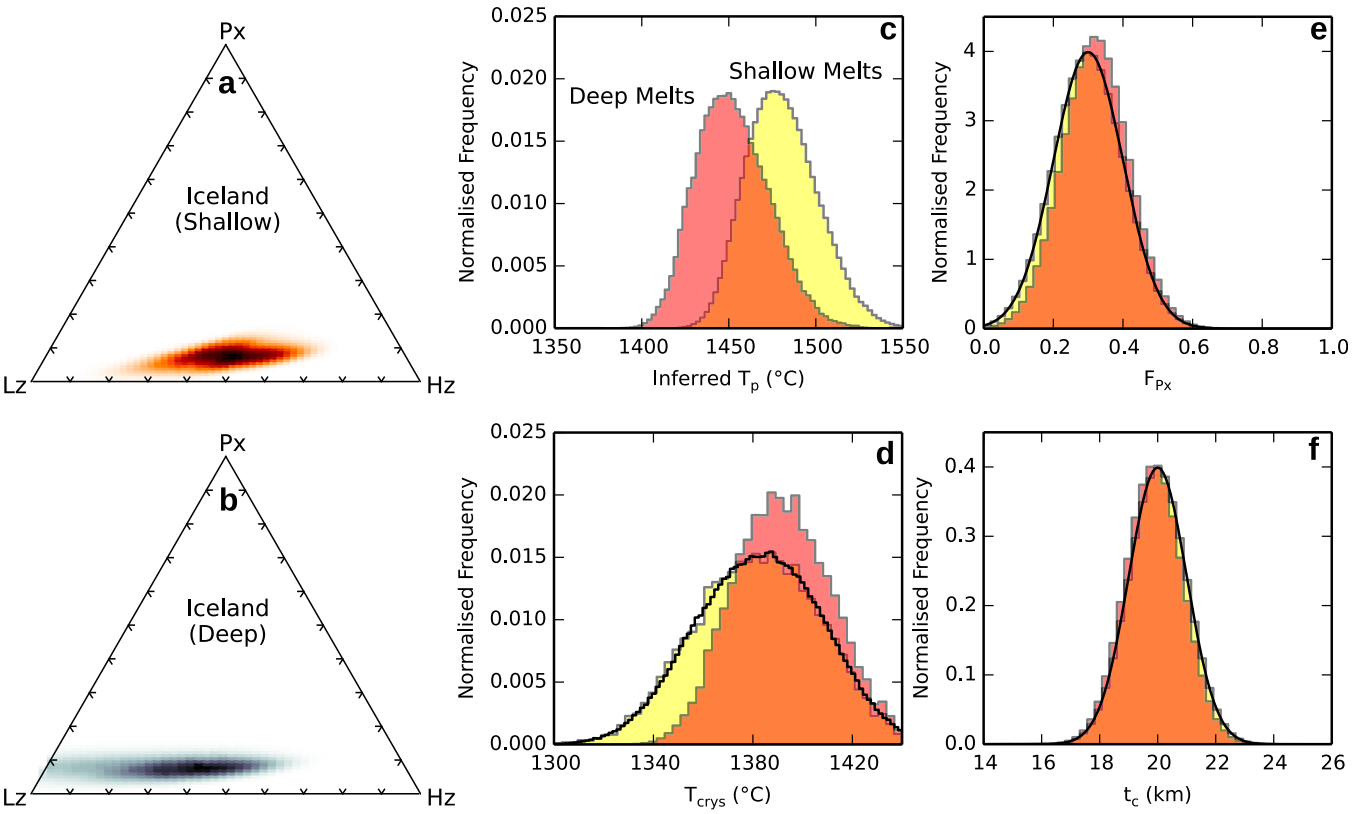

Figure 11. Results from inverting the melting model using observations from Iceland. Two solutions are shown, corresponding to the two end-member cases: highest and lowest T_{crys} for a given T_p, assuming a shallow and deep melt origin, respectively. (a, b) The mantle lithologies (expressed as ϕ_{Px} and ϕ_{Hz}) consistent with the observations. (c) The consistent T_p distributions. The black lines in Figures 11d, 11e, and 11f show the input distributions of T_{crys}, F_{Px}, and t_c, respectively. The filled histograms show the values of each parameter for which solutions were found.

observed t_c. The combination of lower T_p and higher ϕ_{Px} is not compatible with the F_{Px} constraint. This effect is seen only for the solutions for the low T_p (deep melts) bound in Iceland because the solutions for the high T_p (shallow melt) bound have been generated with a higher T_p melting model.

For Siquieros, solutions for the lowest T_{crys} values do not exist for either deep or shallow melts, though this is most pronounced for deep melts. Since the inferred T_p for a given T_{crys} is always lower for the deep melt case, the value of T_p for which 5.7 km of crust can no longer be produced while maintaining F_{Px} occurs at a higher T_{crys} for such melts.

The results of the inversion for Iceland and Siqueiros (MORB) are compared in Figure 1. When T_{crys}, t_c, and F_{Px} constraints are combined, a significantly higher mantle T_p is required to explain the enhanced crustal thickness and higher crystallization temperatures for Iceland compared to Siqueiros. Since no combination of the solutions from high T_p and low T_p bounds allow the same mantle T_p in both the Siqueiros mantle and Icelandic mantle, variation in the depth from which the melts parental to the high T_{crys} are derived cannot explain the difference in T_{crys} between Siqueiros and Iceland. Though different proportions of lherzolite, pyroxenite, and harzburgite are required to fit the observations, variation in lithology alone cannot reproduce the observations. The T_p values inferred from our inversions are consistent with estimates based on REE inversions [*Maclennan et al.*, 2001; *McKenzie and O'Nions*, 1991] and major element chemistry [*Herzberg and Asimow*, 2015]. Though the offset in T_p of MORB and Iceland obtained from the inversion is a similar magnitude to the offset in T_p estimated by *Putirka* [2008a, 2016], our absolute T_p estimates are ~100°C lower.

Results of the same inversion routine, but based on a forward model calculated using a KG1 pyroxenite melting parametrization [*Kogiso et al.*, 1998; *Shorttle et al.*, 2014] in place of the G2 pyroxenite parametrization, are reported and discussed in Appendix B. Using a KG1 pyroxenite results in lower estimates of ϕ_{Hz} but has only a minor effect on estimated T_p.

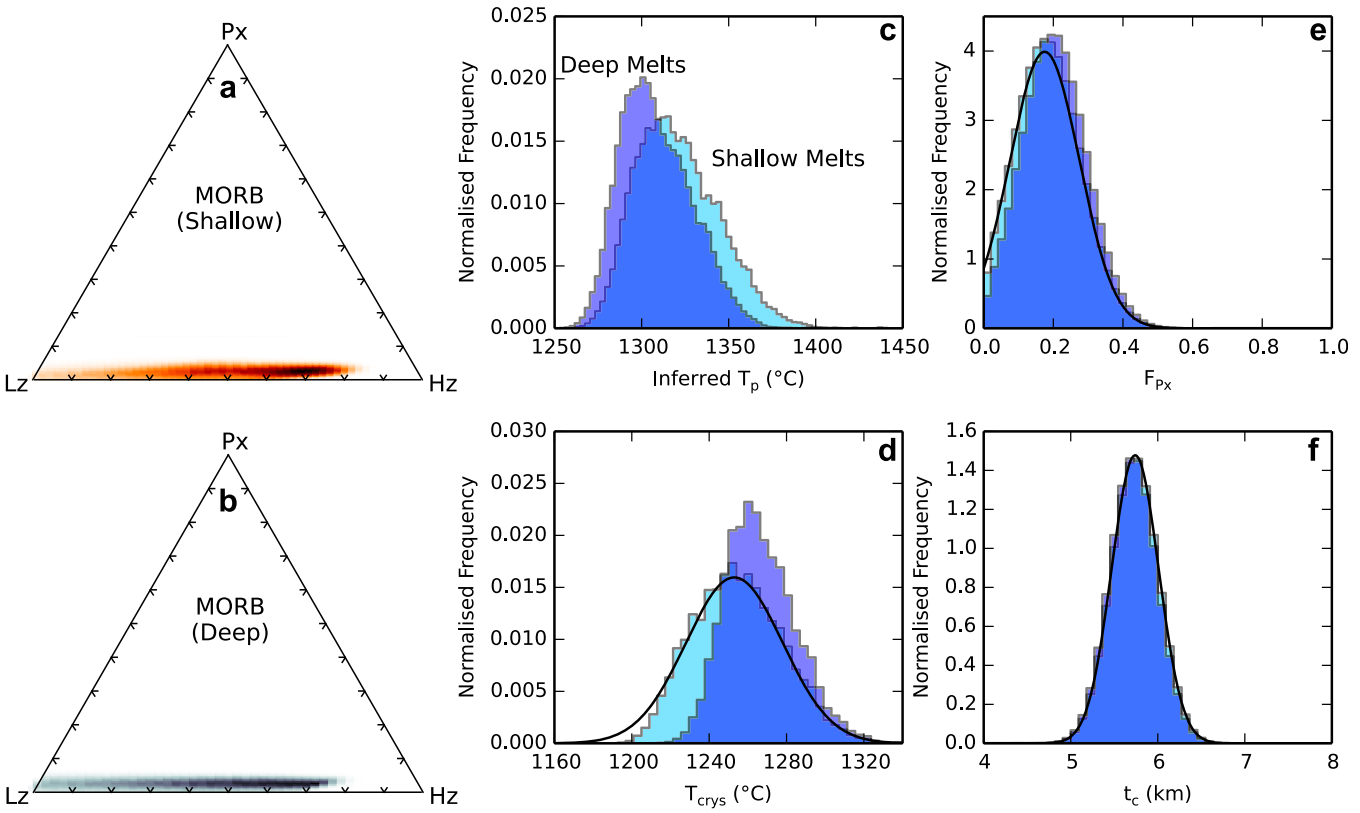

Figure 12. Results from inverting the melting model using observations from Siqueiros. Two solutions are shown, corresponding to the two end-member cases: highest and lowest T_{crys} for a given T_p, assuming a shallow and deep melt origin, respectively. (a, b) The mantle lithologies (expressed as ϕ_{Px} and ϕ_{Hz}) consistent with the observations. (c) The consistent T_p distributions. The black lines in Figures 12d, 12e, and 12f show the input distributions of T_{crys}, F_{Px}, and t_c, respectively. The filled histograms show the values of each parameter for which solutions were found.

6. Discussion

6.1. Olivine-Spinel Al-Exchange Thermometry

The crystallization temperatures measured here for the Northern Volcanic Zone of Iceland are similar to the temperatures for zero-age Iceland measured by *Spice et al.* [2016], though our data set extends the observed range in olivine forsterite content and T_{crys} (Figure 6). The less forsteritic crystals preserve crystallization temperatures similar to the Tertiary crystallization temperatures of *Spice et al.* [2016] at the same forsterite content. The magnitude of temperature variation for these Icelandic olivines is consistent with the fractional crystallization models shown in Figure 6. The olivines that lie furthest from the KR4003 line are from the same eruptions as olivines that lie directly on the line and therefore do not definitively indicate differences in mantle temperature. Instead, these offsets may arise from the presence of diverse melts in deep magma chambers, each with its own liquid line of descent. It is also possible the Mg and Fe content of the olivine has been diffusively reset during mush residence [*Thomson and Maclennan*, 2013], which would change the positions of crystals in forsterite-T_{crys} space. Since it is only the fast-diffusing elements Mg and Fe that are likely to have reequilibrated in the olivine, this process would not affect Al-exchange temperatures.

Table 2. Results From the Inversion (Using G2 Pyroxenite) for Iceland and Siqueiros, for Both Deep and Shallow Melt End-Members[a]

	T_p (°C)	ϕ_{Px}	ϕ_{Hz}
Iceland (Shallow)	1480^{+37}_{-30}	$0.08^{+0.04}_{-0.04}$	$0.47^{+0.16}_{-0.19}$
Iceland (Deep)	1451^{+37}_{-30}	$0.08^{+0.04}_{-0.04}$	$0.35^{+0.22}_{-0.29}$
Siqueiros (Shallow)	1318^{+44}_{-32}	$0.03^{+0.02}_{-0.02}$	$0.54^{+0.21}_{-0.39}$
Siqueiros (Deep)	1306^{+39}_{-27}	$0.03^{+0.02}_{-0.02}$	$0.45^{+0.26}_{-0.28}$

[a]Medians and 95% confidence limits are reported.

The highest crystallization temperatures presented here are from the northernmost part of the Northern Volcanic Zone, while those closest to the plume center, Kistufell and Herubreiartögl [*Shorttle et al.*, 2010], show lower crystallization temperatures. Both Kistufell and Herubreiartögl sample a population of olivine macrocrysts with relatively low forsterite (Figure 5), the lower T_{crys}

estimates are therefore consistent with the olivine macrocrysts being derived from a more evolved parental melt. With the available data, it is therefore not possible to resolve any variation in along-axis mantle T_p within Iceland, highlighting the dangers of interpreting offsets in distributions of crystallization temperature.

A more reliable indicator of T_p variation is the offset in T_{crys} at fixed olivine forsterite content, as this must represent a difference in the composition of melt leaving the mantle. As discussed in section 5.4, such a difference in melt composition, and therefore T_{crys}, can arise from both a difference in mantle T_p and mantle lithology. Although there is little offset in T_{crys} between the zero-age Iceland data (from this study and *Spice et al*. [2016]) and the Tertiary Iceland data [from *Spice et al*., 2016], secular change in the temperature of the Icelandic mantle cannot be ruled out since mantle T_p can vary without changing T_{crys} (section 5.4). Instead the style of melt extraction or composition of the mantle may change to offset the change in T_p.

6.2. Thermal Equilibration

In calculating the forward model, thermal equilibrium is assumed in the solid matrix. *Phipps Morgan* [2001] and *Katz and Rudge* [2011] argue this is a reasonable assumption as long as the heterogeneities have a length scale of <1 km. Though this is likely to be the case, considering combinations of end-member lithologies means the model can still be applied if it is not, but it will no longer be applicable to predicting properties sensitive to the bulk melting region, for example t_c and F_{Px}. Melts are likely to approach thermal equilibrium with the mantle through which they pass, and therefore the bound on T_p given by the deepest melts is likely unrealistically low. However, perturbations from the model geotherm in the melting region arising from channelization reactions and advection of heat by rising magma could allow melts to equilibrate at higher temperatures than the modeled geotherm. Since the effects of these processes are poorly constrained, we assume maximum possible disequilibrium, i.e., melts follow the liquid adiabat to the magma chamber. By using such conservative bounds, the uncertainty in the thermal history during melt transport can be fully propagated.

6.3. Melting Parameterizations

The melting behavior of the lithological end-members must be assumed when constructing the model. In addition to G2 pyroxenite, *Shorttle et al*. [2014] also describe the behavior of the melting model for a pyroxenite formed from a mixture of MORB and lherzolite, KG1 [*Kogiso et al*., 1998], after *Shorttle and Maclennan* [2011] found that melts from such a lithology provided a good fit to the chemistry of enriched basalts. The melting behavior of these two pyroxenites differ in the position of their solidii (G2 begins melting at higher pressure) and their productivity, $\frac{dF}{dP}$, beyond the solidus (G2 is more productive). Using the G2 parametrization over the KG1 parametrization in our model has the effect of increasing the temperature of first melt generation (and therefore the upper crystallization temperature bound) and increasing the melt fraction, increasing the t_c estimate and reducing the temperature in the melting region. Using the G2 melting parametrization therefore makes the T_{crys} bounds more conservative. As we show in Appendix B, the choice of pyroxenite parametrization has only a small effect on inferred T_p.

We assume the harzburgite component will not undergo melting, which may not be true; indeed the lherzolite parametrization includes an interval of melting after clinopyroxene exhaustion when the residue is harzburgitic. However, the extent of harzburgite melting will be very small, or zero for modest ϕ_{Hz}, and will begin significantly after the onset of both lherzolite and pyroxenite melting. This assumption therefore has no effect on the high T_{crys} bound, and only a very minor effect on the position of the low T_{crys} bound and predicted t_c.

Since the melting parameterizations employed here are not necessarily realistic for the Icelandic mantle, the results of the inversion for composition must be interpreted with care. In particular, how the inferred harzburgite component should be interpreted is unclear. The effect of adding harzburgite could be replicated by changing other properties of the mantle. Since including harzburgite decreases the bulk melt productivity, a high ϕ_{Hz} may imply the lherzolite and pyroxenite components are less productive than modeled. This is borne out by the lower ϕ_{Hz} estimate resulting from using a less fusible pyroxenite model (Appendix B). Incorporating the harzburgite component not only is required to satisfy plume buoyancy constraints [*Shorttle et al*., 2014] but also allows the model to accommodate variations in mantle fusibility without affecting estimated T_p (though the relative fusibilities of lherzolite and pyroxenite are fixed, and control the

effect of the F_{Px} constraint). Though the melting parametrizations are used to model fractional melting, they are based on batch melting experiments; the addition of a harzburgite component will compensate for overestimates of melting productivity resulting from this [*Stolper and Asimow*, 2007].

In application of both the lherzolite and pyroxenite parameterizations, we assume that no hydrous melting takes place. When a small amount of water or carbon is present in the upwelling mantle, melting begins earlier and at higher temperature [*Wyllie*, 1975; *Canil and Scarfe*, 1990; *Dasgupta and Hirschmann*, 2006], resulting in an increased high T_{crys} bound. However, the effect on bulk melt production (and therefore the low T_{crys} bound and t_c estimate) is very small since only very small melt fractions are produced during this phase of volatile-present melting. These very first, highly volatile and incompatible trace element-enriched, melts have never been seen in melt inclusions and so are unlikely to move far in the mantle before reacting or mixing with other higher-volume melts [*Rudge et al.*, 2013]. While the current high T_{crys} bound suffers from the same argument it is unclear where the deepest depth of equilibration should be, and so the high T_{crys} bound is rather conservative.

6.4. Crystallization Depth

A depth of crystallization must be assumed when calculating the basalt liquidus temperature. In all models presented here it is taken to be the base of the crust, as calculated from the melting model. Barometry on high-Mg# clinopyroxene crystals from wehrlite nodules in Borgarhraun by *Winpenny and Maclennan* [2011] indicates that erupted clinopyroxenes crystallized near or below the Moho at 20–25 km. Since the olivine crystals used in our inversion are all highly forsteritic and petrographically similar to the olivine found in the wehrlitic nodules, they are likely to be part of this deep population. Though crystallization depth is unconstrained for the Siqueiros olivines, the uncertainty arising from crystallization depth (less than 10°C for Borgarhraun) is much smaller than the uncertainty in the thermometer calibration and the uncertainty in the thermal history of the melt.

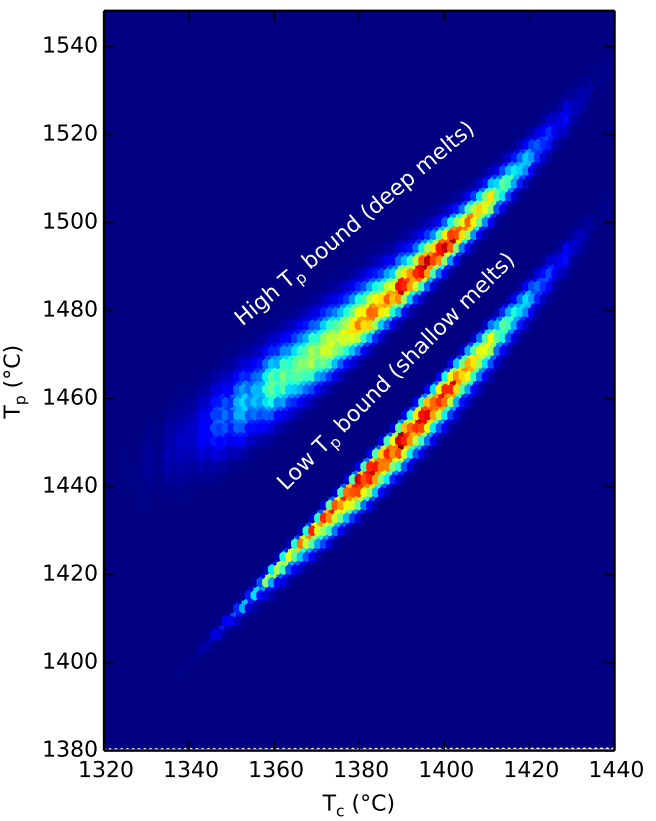

Figure 13. Histogram showing the relationship between T_p estimate and T_{crys} for the Iceland inversion. Both the upper and lower T_p bounds are shown. Brightness corresponds to density of results.

6.5. Inferring Mantle T_p

For a single value of T_{crys}, the model predicts a large range of consistent T_p, 170°C for $T_{crys} = 1385$°C (Figure 10), suggesting a very large offset in primitive crystal T_{crys} is required before a difference in T_p can be robustly inferred from thermometry alone. When the range of solutions can be constrained using other parameters, t_c and F_{Px} in this case, a much narrower range in consistent T_p can be identified. Figure 13 shows the uncertainty in this inversion propagates mostly from the uncertainty in T_{crys} and melt source depth.

The subset of solutions consistent with the t_c and F_{Px} constraints has T_p distributions (Figure 1) that coincide with those estimated using other techniques and observations. Since t_c is an integral part of the inversion, it is not surprising that the inversion yields similar answers to studies that have fitted melting models to t_c observations, though in general such models do not allow the source composition to vary.

Brown and Lesher [2014] do allow pyroxenite fraction to vary in their

model but do not consider the effect of harzburgite. Without a harzburgite fraction, the bulk productivity of a mantle containing only lherzolite and pyroxenite will be greater. The greater mantle productivity, in addition to a small component of active upwelling, allows the same pyroxenite fraction and crustal thickness observations to be matched with a slightly lower T_p than both *Shorttle et al*. [2014] and our shallow melt solution. *Brown and Lesher* [2014] infer higher T_p in central Iceland in order to match the thicker crust and basalt Nd-isotope geochemistry. Their model achieves thicker crust by increasing both the melt fraction and the degree of active upwelling, both a consequence of higher mantle T_p. We do not consider crustal thickness observations from central Iceland, or active upwelling here, for the reasons set out in section 5.3.

The analysis presented here shows that T_p inferred from T_{crys} estimates can be reconciled with T_p estimates derived from other observations, whereas those presented by *Putirka* [2005] are systematically higher. The origin of this discrepancy is discussed in Appendix A.

The positions of the T_p distributions estimated for Iceland (Figure 1) show a small offset between the shallow and deep melt solutions; however, it is the shallow melt distribution that shows the closest correspondence to other T_p estimates. This similarity suggests that the highest T_{crys} observations come from melts derived from the shallow parts of the melting region. Measurements of olivine-hosted melt inclusions from Borgarhraun [*Maclennan et al*., 2003] show that the most highly forsteritic olivines in Borgarhraun have trapped melts with exceptionally low La/Yb, also suggesting the parental melts originated shallow in the melting region. Within both the MORB and Iceland data sets there is approximately 150°C variation in crystallization temperature for primitive olivine crystals. As shown in Figure 9 this is a similar magnitude to the predicted range in crystallization temperature for lithology combinations with moderate amounts of pyroxenite and harzburgite. However, this would imply the crystals preserving the highest T_{crys} are derived from the deepest melts, contrary to that implied by the correspondence of T_{crys} estimates and melt inclusion measurements made in highly forsteritic Borgarhraun macrocrysts.

7. Conclusions

We have obtained new crystallization temperature estimates for four eruptions in the Northern Volcanic Zone of Iceland using the *Coogan et al*. [2014] Al-exchange thermometer. The maximum crystallization temperature we calculated is 1399°C, substantially higher than the maximum crystallization temperature in the *Coogan et al*. [2014] MORB data set of 1270°C. To explore the mantle controls on crystallization temperature, we developed a thermal model of mantle melting, and used this to quantify the uncertainties in converting crystallization temperature to mantle potential temperature. The uncertainties considered in the model arise from uncertainties in mantle lithology and the thermal history of melts after they have been generated. When crystallization temperature is the only observation used to constrain mantle potential temperature, the maximum crystallization temperature for Iceland can be satisfied by a mantle potential temperature as low as 1385°C and in excess of 1550°C, depending on the parental melt's depth of origin. We used crustal thickness and the fraction of bulk crust derived from pyroxenitic melts to constrain the mantle potential temperature further, yielding an estimate for T_p of 1480^{+37}_{-30} °C for Iceland and 1318^{+44}_{-32} °C for Siqueiros. These mantle potential temperature estimates are consistent with estimates derived using other techniques.

Appendix A: The Discrepancy Between Olivine-Spinel Al-Exchange Thermometry and Olivine-Liquid Mg-Fe Exchange Thermometry

A1. Iceland

There exists a 100°C discrepancy between the estimated T_p for Iceland in this study and that by *Putirka* [2008a], despite both being based on observations of the Borgarhraun lava flow. This discrepancy arises due to an elevated estimate of olivine-liquid equilibration temperature and from the magnitude of the latent heat of melting correction used by *Putirka* [2008a], as illustrated in Figure A1.

A key parameter used in calculating the magnitude of the latent heat of melting correction is the melt fraction. The melt fraction estimated by *Putirka* [2008a] is similar to that estimated here (Figure A1b), therefore the larger latent heat of melting correction applied by *Putirka* [2008a] originates from using different thermodynamic constants. However, this explains only 44°C of the total T_p discrepancy.

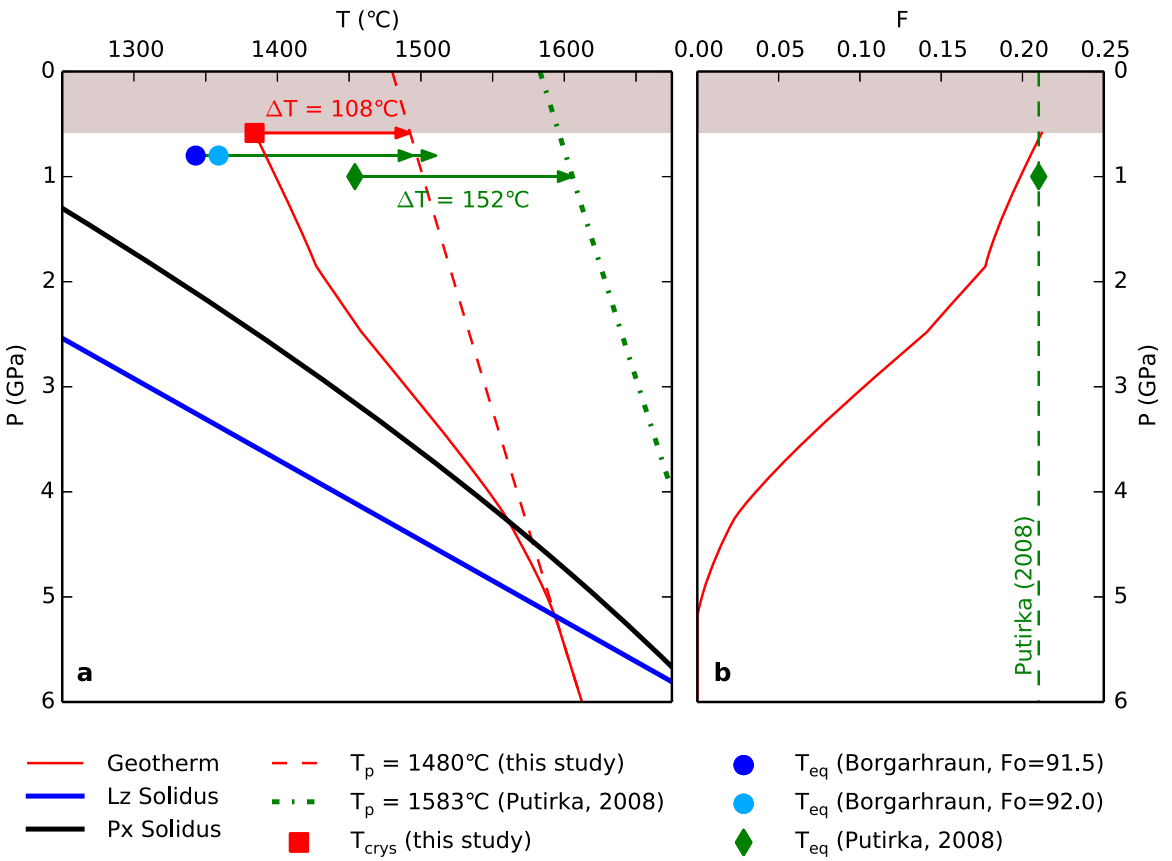

Figure A1. (a) The calculated geotherm for the best-fit model for Iceland found by our inversion. The red arrow indicates the magnitude of the correction for the heat of fusion we calculate. The green diamond shows the pressure and temperature of olivine-liquid equilibration calculated by *Putirka* [2008a] for Iceland, and the green arrow the magnitude of the heat of fusion correction he applies. The blue circles indicate olivine-liquid Mg-Fe equilibration conditions calculated in this study for Borgarhraun; the green arrows connecting to them show the same heat of fusion correction as *Putirka* [2008a]. (b) The melt fraction calculated along the best-fit geotherm, and that calculated by *Putirka* [2008a] for Iceland. Shading indicates the crustal thickness.

The olivine-liquid equilibration temperature estimated by *Putirka* [2008a] relies on using a compilation of whole-rock major element data to infer the composition of melt in equilibrium with Fo_{92} olivine. The temperature dependence of Mg-Fe partitioning between olivine and melt is then used to estimate the equilibration temperature. *Keiding et al*. [2011] and *Herzberg* [2011] suggest incomplete mixing of fractional melts leads to overestimation of the FeO concentration in the magma that equilibrated with the highest forsterite olivine. *Shorttle and Maclennan* [2011] demonstrate such major element diversity is observed in whole-rock geochemistry in Iceland. Figure A2 shows chemical data from a compilation of northern Northern Volcanic Zone whole-rock analyses. La/Yb ratios are a measure of geochemical enrichment and show a clear positive correlation with FeO (total FeO, assuming all Fe is ferrous), as described by *Shorttle and Maclennan* [2011]. Much of this range is seen in olivine-hosted melt inclusions found in the Borgarhraun lava flow [*Maclennan et al*., 2003]. The most forsteritic olivine crystals have trapped the most depleted (lowest La/Yb) melts exclusively, and their La/Yb is indicated by the vertical line in Figure A2a. We therefore argue that only the most FeO-poor melts are likely to have been in equilibrium with Fo_{92} olivine.

Table A1. Major Element Composition of Melts (wt %) Used to Calculate Olivine-Melt Mg-Fe Exchange Temperatures for Iceland in This Study and by *Putirka et al*. [2007][a]

	Fo (mol %)	SiO_2	TiO_2	Al_2O_3	FeO	Fe_2O_3	MnO	MgO	CaO	Na_2O	K_2O
Putirka et al. [2007]	92	47.2	0.7	12.3	7.8	1.7	0.2	18.2	10.5	1.4	0.1
Borgarhraun	91.5	48.9	0.6	14.2	7.1	1.4	0.2	13.2	12.6	1.6	0.05
Borgarhraun	92	48.7	0.7	13.9	7.1	1.4	0.2	14.2	12.3		0.05

[a]Compositions calculated by finding equilibrium with the olivine composition indicated, as described in the text. FeO and Fe_2O_3 reported on the basis of a Fe^{3+}/FeO of 0.16 [*Óskarsson et al*., 1994]

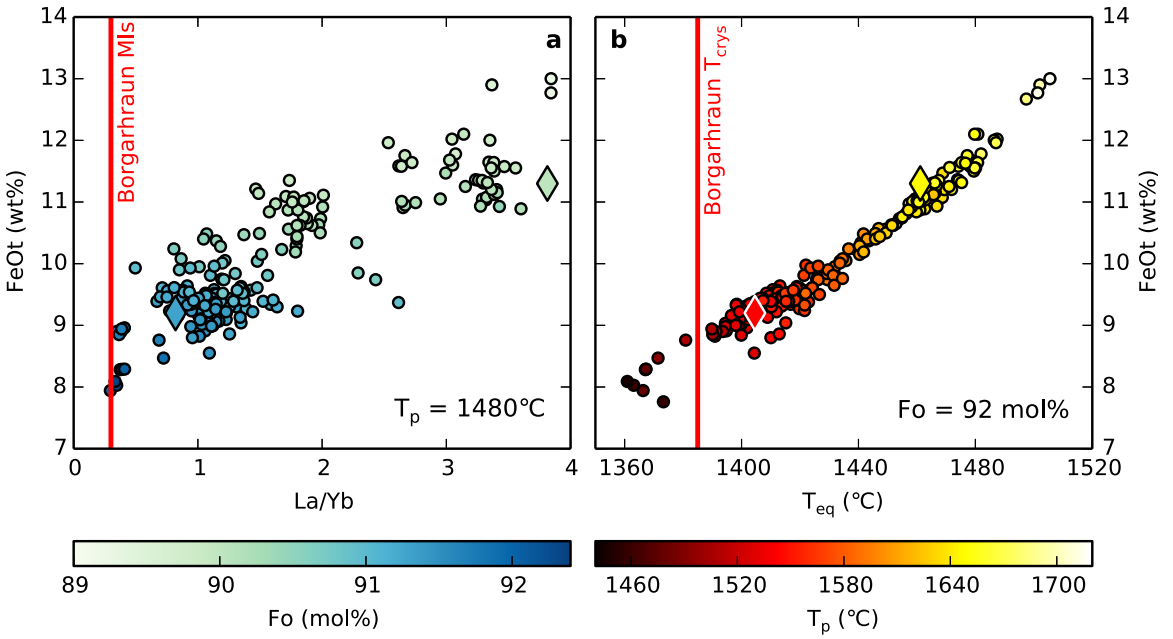

Figure A2. (a) Whole-rock chemical data for basalts with MgO >8 wt % from the northern part of the Northern Volcanic Zone of Iceland. The La/Yb ratio found in the most forsteritic melt inclusions from Borgarhraun is indicated by the vertical line. The color indicates the olivine composition calculated to be in equilibrium with the estimated parental melt for a mantle of T_p = 1480°C. (b) The calculated temperature of olivine-liquid equilibration as a function of melt composition, assuming the estimated parental melts are in equilibrium with Fo_{92} olivine at 0.8 GPa. The colors show the mantle T_p calculated using the method of *Putirka et al*. [2007]. The vertical line indicates the crystallization temperature we estimate for Borgarhraun using olivine-spinel aluminum exchange thermometry. In both plots, the diamonds indicate the depleted and enriched end-members identified by *Shorttle and Maclennan* [2011]. Data from *Nicholson et al*. [1991], *Hémond et al*. [1993], *Hardarson et al*. [1997], *Maclennan et al*. [2001], *Skovgaard et al*. [2001], *Slater et al*. [2001], *Maclennan et al*. [2003], *Stracke et al*. [2003b], *Kokfelt et al*. [2006], *Peate et al*. [2010], and *Sims et al*. [2013].

To test the effect of using an FeO-poor melt on the calculated olivine-liquid equilibration temperature we estimate the composition of the melt parental to average Borgarhraun whole rock [*Maclennan et al*., 2003] by adding olivine until equilibrium with a chosen olivine composition is reached (Table A1). This is analogous to the regression employed by *Putirka* [2005], *Putirka et al*. [2007], and *Putirka* [2008a, 2016]. We use *Putirka et al*. [2007, equation (4)], and equilibrate with Fo_{92} olivine [after *Putirka*, 2008a] and $Fo_{91.5}$ olivine (the most forsteritic olivine analyzed in this study). The equilibration pressure is assumed to be 0.8 GPa [after *Winpenny and Maclennan*, 2011], the exchange partition coefficient as 0.31 [after *Putirka*, 2008a], and the ferric/total iron ratio as 0.16 [after *Óskarsson et al*., 1994; *Shorttle et al*., 2015]. The resulting estimates are shown as blue circles in Figure 2 and are close to the Al-exchange temperature, though slightly lower. When the *Putirka* [2008a] latent heat of melting correction is applied a similar mantle T_p to that calculated in this study is found (Figure A1a).

This effect is tested further by calculating the olivine-melt equilibration temperature for each composition in the northern Northern Volcanic Zone data set. The same methodology as we applied to the Borgarhraun whole-rock composition is employed here, setting the olivine composition as Fo_{92}. The results are shown in Figure A2b. The vertical line on the figure shows the Al-exchange temperature for highly forsteritic olivine reported in this study, demonstrating that this method is in agreement with temperatures calculated using Mg-Fe exchange provided a melt with low FeO is used. The estimated temperature drop during melting from the latent heat of fusion was estimated using the method of *Putirka et al*. [2007], where melt fraction was calculated using his equation (A1). The color in Figure A2b indicates the corresponding T_p estimate, with those calculated for the lowest FeO compositions in agreement with our estimate.

Much of the range of whole-rock compositions from the northern Northern Volcanic Zone was found by *Shorttle and Maclennan* [2011] to represent mixed, but not fractionated, mantle melts. They should therefore be consistent with a single mantle T_p but may reflect variable melt fraction and mantle olivine composition. To test this hypothesis, the required olivine composition to be consistent with a T_p = 1480°C mantle was calculated for each melt in the data set. Olivine was added to each melt until the calculated T_p was equal to 1480°C, with a new latent heat of melting correction calculated for the new liquid composition at each step.

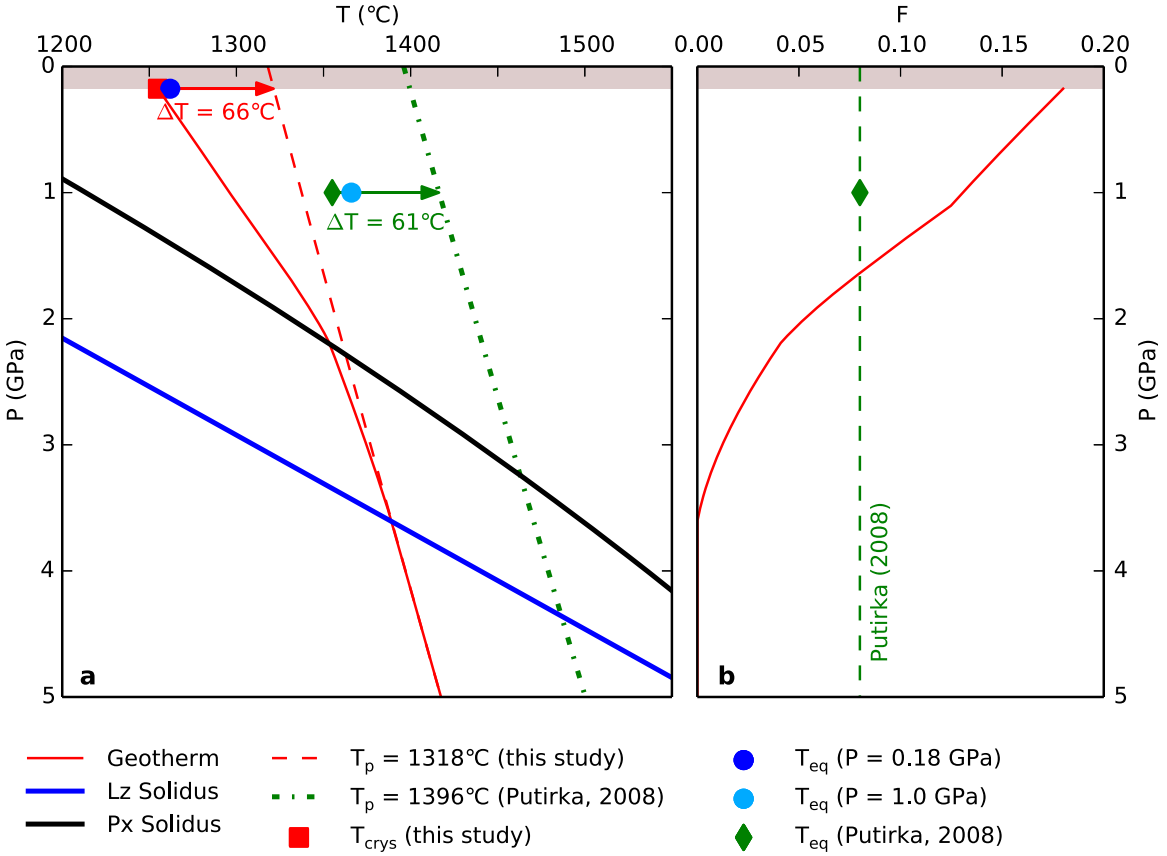

Figure A3. (a) The calculated geotherm for the best-fit model for Siqueiros found by our inversion. The red arrow indicates the magnitude of the correction for the heat of fusion we calculate. The green diamond shows the pressure and temperature of olivine-liquid equilibration calculated by *Putirka* [2008a] for Siqueiros, and the green arrow the magnitude of the heat of fusion correction he applies. The blue circles indicate olivine-liquid Mg-Fe equilibration conditions calculated in this study for Siqueiros using the primary melt composition inferred by *Putirka* [2008a], with olivine added until it is in equilibrium with $Fo_{91.5}$ olivine at the pressure of interest. (b) The melt fraction calculated along the best-fit geotherm and that calculated by *Putirka* [2008a] for Siqueiros. Shading indicates the crustal thickness.

Fo_{92} olivine was obtained for the lowest FeO melts, while Fo_{90} was calculated for the more FeO rich (and trace element-enriched) melts. This is consistent with the absence of enriched (high La/Yb) melt inclusions in Borgarhraun olivines more forsteritic than Fo_{90}.

A2. Siqueiros

A discrepancy of 80°C exists between the Siqueiros mantle T_p inferred here and by *Putirka* [2008a]. Figure A3 demonstrates how the discrepancy arises from the 100°C difference in temperature estimate from olivine-spinel Al-exchange thermometry [*Coogan et al.*, 2014] and olivine-melt Mg-Fe exchange thermometry [*Putirka*, 2008a]. *Coogan et al.* [2014] argue this difference arises via incomplete mixing of mantle melts in much the same way as we suggest for Iceland, and was previously suggested by *Keiding et al.* [2011] and *Herzberg* [2011]; however, coexisting olivine and glass are in Mg# equilibrium in Siqueiros rocks [*Putirka et al.*, 2007]. Instead, we propose the discrepancy arises from our differing assumptions about olivine-liquid and olivine-spinel equilibration pressure. In the inversions presented here, the temperature recorded by the Al-exchange thermometer is assumed to represent the temperature of melts crystallizing at the base of the crust, at a pressure of 0.18 GPa. In contrast, *Putirka* [2008a] assume an olivine-melt equilibration pressure of 1 GPa. In our calculation of mantle T_p, pressure is needed only to calculate T_p once a temperature on the solid adiabat has been estimated (except for the deep melts end-member when it is also required to estimate the liquidus temperature at low pressure, as illustrated in Figure 7). However, the method employed by *Putirka* [2005], *Putirka et al.* [2007], and *Putirka* [2008a, 2016] requires an assumption about equilibration pressure to extract a temperature estimate from the olivine-liquid equilibrium, in addition to calculating T_p once a temperature on the solid adiabat has been estimated.

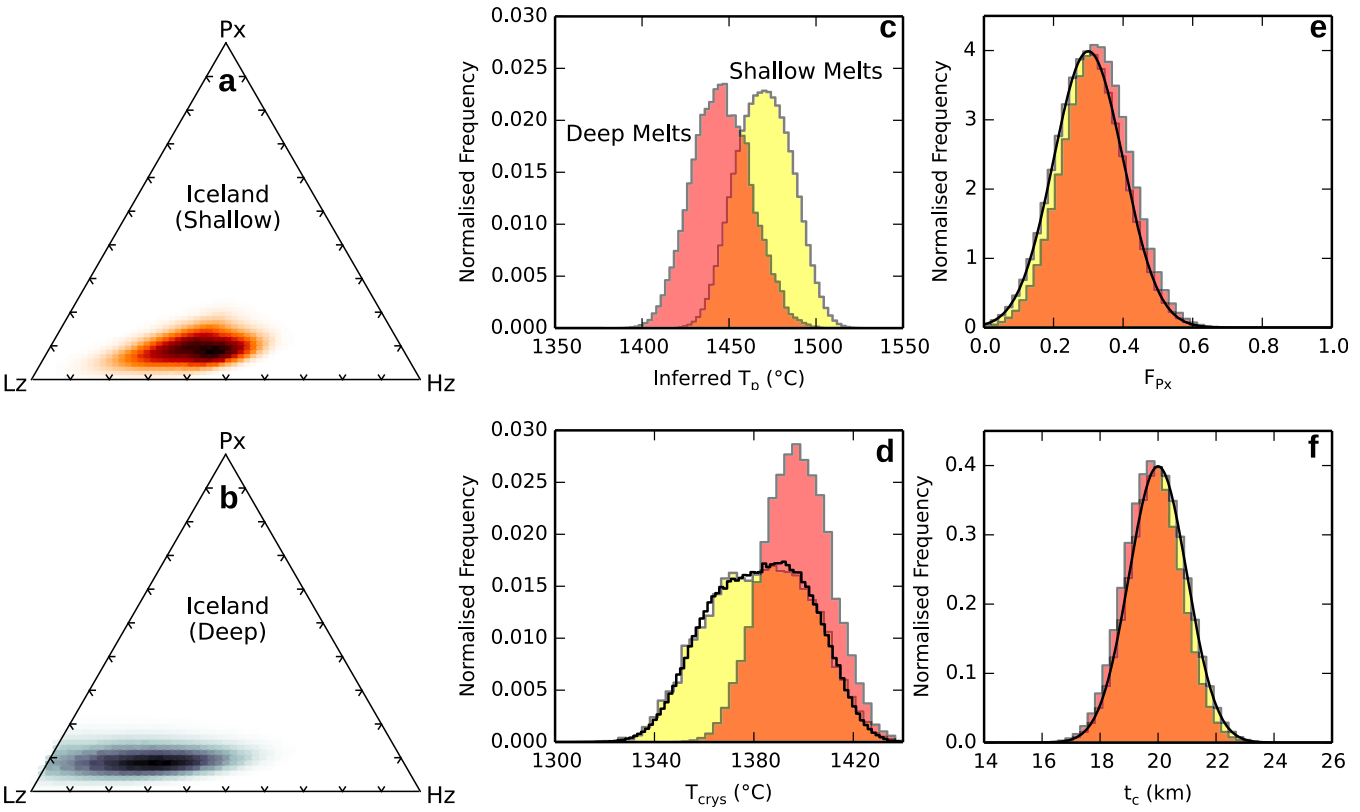

Figure B1. Results from inverting the KG1 pyroxenite melting model using observations from Iceland. Two solutions are shown, corresponding to the two end-member cases: highest and lowest T_{crys} for a given T_p, assuming a shallow and deep melt origin, respectively. (a, b) The mantle lithologies (expressed as ϕ_{Px} and ϕ_{Hz}) consistent with the observations. (c) The consistent T_p distributions. The black lines in Figures B1d, B1e, and B1f show the input distributions of T_{crys}, F_{Px}, and t_c, respectively. The filled histograms show the values of each parameter for which solutions were found.

To test the effect of pressure assumptions on olivine-liquid Mg-Fe exchange temperature estimate, we use the method outlined above to estimate this temperature for the pressure at the base of the Siqueiros crust. Following *Putirka* [2008a], we allow the melt to equilibrate with Fo $_{91.5}$ olivine by addition of olivine. Though the melt composition is inferred on the basis of Fo $_{91.5}$ equilibrium, this step ensures consistency with our choice of parameters. We calculate a olivine-liquid Mg-Fe exchange temperature of 1262°C, shown by the dark blue circle in Figure A3a, which is extremely close to the maximum *Coogan et al.* [2014] Al-exchange temperature. In order to show our choice of calculation parameters is not responsible for this different Mg-Fe exchange temperature estimate, we repeat the procedure for 1.0 GPa (light blue circle in Figure A3a). Though our choice of parameters does result in a small discrepancy, the effect is a bias toward higher equilibration temperature estimates. We argue 0.18 GPa is a more appropriate choice for the pressure of melt-liquid equilibration, assuming either equilibration during crystallization or during mantle melting/transport. Though one of the bounds of our model assumes melt-mantle equilibration at the base of the melting region, we do not apply a correction for the latent heat of fusion in this case. If the melt was in equilibrium with mantle olivine at 1 GPa prior to extraction, the latent heat of fusion correction should represent the melt fraction at that depth. While it is possible that the melt fraction calculated by *Putirka* [2008a] reflects the melt fraction at this depth, there is a clear discrepancy with the melt fraction-pressure curve we calculate (Figure A3b).

In further contrast to the Iceland discrepancy, the corrections for the temperature lost during melting due to the latent heat of fusion calculated in this study and by *Putirka* [2008a] differ only by 5°C. The lower melt fraction estimate by *Putirka* [2008a] counteracts the effect of differing choice of thermodynamic parameters. In summary, if the melt-olivine equilibration pressure is set to 0.18 GPa, Al-exchange and Mg-Fe exchange thermometry are consistent for Siqueiros.

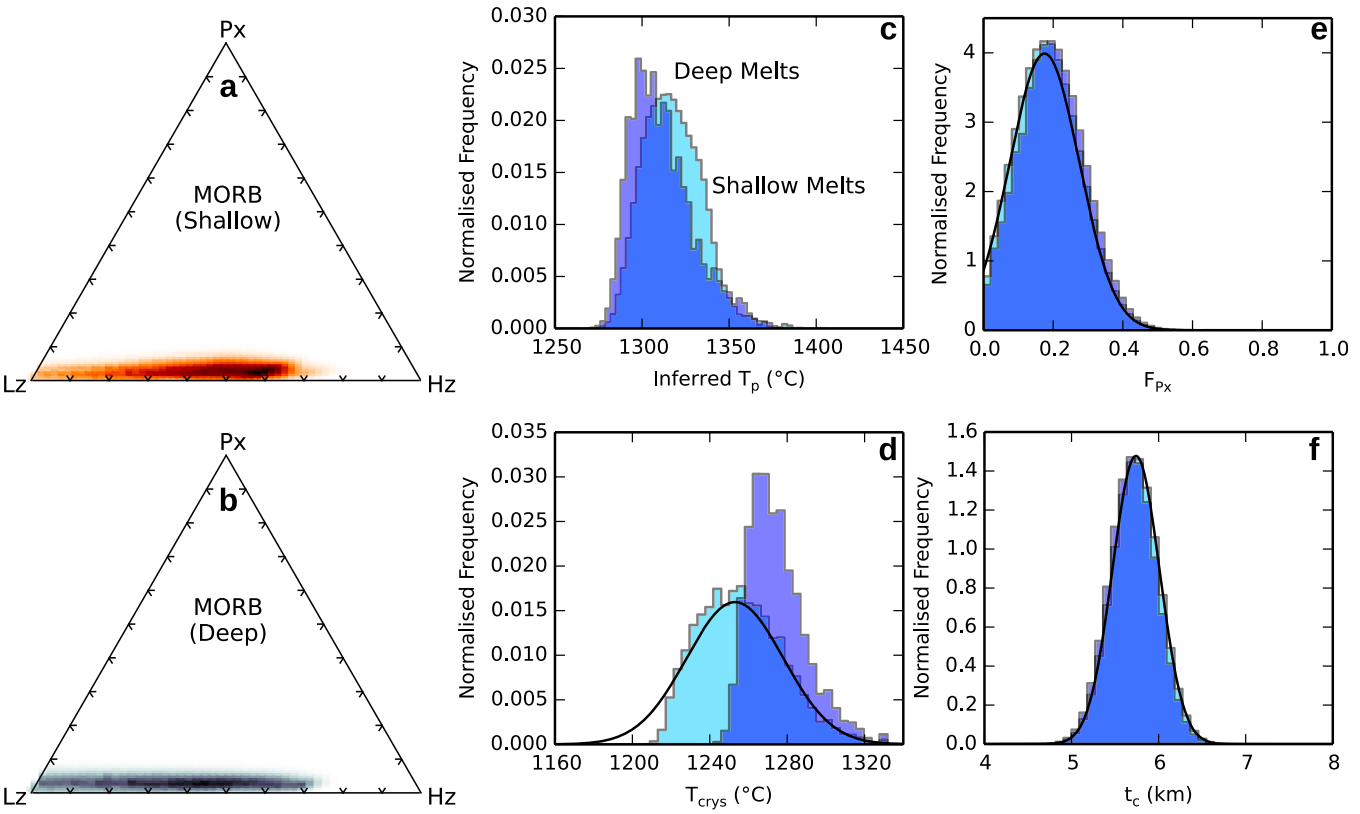

Figure B2. Results from inverting the KG1 pyroxenite melting model using observations from Siqueiros. Two solutions are shown, corresponding to the two end-member cases: highest and lowest T_{crys} for a given T_p, assuming a shallow and deep melt origin, respectively. (a, b) The mantle lithologies (expressed as ϕ_{Px} and ϕ_{Hz}) consistent with the observations. (c) The consistent T_p distributions. The black lines in Figures B2d, B2e, and B2f show the input distributions of T_{crys}, F_{Px}, and t_c, respectively. The filled histograms show the values of each parameter for which solutions were found.

Appendix B: Inversion Using the KG1 Pyroxenite Melting Model

Shorttle and Maclennan [2011] estimated the major element composition of the enriched end-member melt in Iceland and found it to be very close to the composition of experimental melts of KG1 pyroxenite [*Kogiso et al.*, 1998]. A parametrization of the melting behavior of KG1 was provided by *Shorttle et al.* [2014] and can be implemented in place of G2 pyroxenite [*Pertermann and Hirschmann*, 2003] in the melting model presented here. The two models differ in the position of their solidii (KG1 melts at higher temperature), and their productivity (KG1 is less productive). The G2 pyroxenite therefore represents a good end-member for the behavior of pyroxenite; it melts at a much lower temperature and is extremely productive compared to KLB-1-like lherzolite. We choose to discuss the behavior of the G2 model in the main text for this reason, and so our conclusions are more robust.

Results of the inversion for Iceland and Siqueiros are given in Table B1 and shown in Figures B1 and B2, respectively. For the low T_p (deep melts) bound of the Iceland inversion, no solutions were found for the lowest values of T_{crys}, similar to the G2 Model inversion. For Siqueiros solutions for the lowest T_{crys} values do not exist for either deep or shallow melts, though this is most pronounced for deep melts. The same effect is seen in the G2 inversion results. The distributions of T_p estimate are very similar to those calculated by inverting the melting model containing G2 pyroxenite (Figures 11 and 12). A bigger difference is seen in the estimates of ϕ_{Hz} which are considerably

Table B1. Results From the Inversion (Using KG1 Pyroxenite) for Iceland and Siqueiros, for Both Deep and Shallow Melt End-Members[a]

	T_p (°C)	ϕ_{Px}	ϕ_{Hz}
Iceland (Shallow)	1470^{+32}_{-29}	$0.09^{+0.06}_{-0.05}$	$0.38^{+0.15}_{-0.19}$
Iceland (Deep)	1448^{+40}_{-28}	$0.09^{+0.06}_{-0.05}$	$0.26^{+0.24}_{-0.22}$
Siqueiros (Shallow)	1316^{+29}_{-24}	$0.03^{+0.03}_{-0.02}$	$0.44^{+0.20}_{-0.34}$
Siqueiros (Deep)	1309^{+39}_{-21}	$0.03^{+0.02}_{-0.02}$	$0.36^{+0.30}_{-0.31}$

[a]Medians and 95% confidence limits are reported.

lower. A decrease in ϕ_{Hz} results in a less refractory bulk mantle, harzburgite fraction trades off against pyroxenite fusibility.

Though the results of the inversion are influenced by the choice of pyroxenite lithology, the effect on estimated T_p is comparatively small. We argue, therefore, our mantle temperature estimates are robust against the uncertainty in choice of pyroxenite melting model. Less robust are the calculated lithology fractions.

Acknowledgments
Supporting information Table S1 contains average chemical data and thermometry results for each crystal pair studied. The authors thank A. Thomson and L. Tweed for preparing sample mounts, E. Jennings and J. Rudge for helpful discussions about Al-exchange thermometry and the thermal model, and I. Buisman for her assistance with the EPMA analyses. G. Fitton, K. Putirka, and E. Brown are thanked for their insightful reviews of the manuscript. In addition, informal reviews from M. Hartley and D. Neave greatly improved the text. S.M. was supported by a Natural Environment Research Council Studentship (NE/L002507/1 and NE/M000427/1). J.M. was supported by a Natural Environment Research Council grant (NE/J021539/1). O.S. was supported by a Title A Fellowship from Trinity College Cambridge and a Geology Option Postdoctoral Fellowship at Caltech.

References

Aghaei, O., M. R. Nedimović, H. Carton, S. M. Carbotte, J. Pabelo Canales, and J. C. Mutter (2014), Crustal thickness and Moho character of the fast-spreading East Pacific Rise from 9°42′N to 9°57′N from poststack-migrated 3-D MCS data, *Geochem. Geophys. Geosyst.*, *15*, 634–657, doi:10.1002/2013GC005069

Beattie, P. (1993), Olivine-melt and orthopyroxene-melt equilibria, *Contrib. Mineral. Petrol.*, *115*, 103–111, doi:10.1007/BF00712982.

Breddam, K. (2002), Kistufell: Primitive melt from the Iceland mantle plume, *J. Petrol.*, *43*(2), 345–373, doi:10.1093/petrology/43.2.345.

Brown, E. L., and C. E. Lesher (2014), North Atlantic magmatism controlled by temperature, mantle composition and buoyancy, *Nat. Geosci.*, *7*, 820–824, doi:10.1038/ngeo2264.

Canil, D., and C. M. Scarfe (1990), Phase relations in the peridotite + CO_2 systems to 12 GPa: Implications for the origin of kimberlite and carbonate stability in the Earth's upper mantle, *J. Geophys. Res.*, *95*, 15,805–15,816, doi:10.1029/JB095iB10p15805.

Chauvel, C., and C. Hémond (2000), Melting of a complete section of recycled oceanic crust: Trace element and Pb isotopic evidence from Iceland, *Geochem. Geophys. Geosyst.*, *1*(2), 1001, doi:10.1029/1999GC000002.

Coogan, L. A., A. D. Saunders, and R. N. Wilson (2014), Aluminium-in-olivine thermometry of primitive basalts: Evidence of an anomalously hot mantle source for large igneous provinces, *Chem. Geol.*, *368*, 1–10, doi:10.1016/j.chemgeo.2014.01.004.

Danyushevsky, L. V., and P. Plechov (2011), Petrolog3: Integrated software for modeling crystallization processes, *Geochem. Geophys. Geosyst.*, *12*, Q07021, doi:10.1029/2011GC003516.

Darbyshire, F. A., I. T. Bjarnason, and Ó. G. Flóvenz (1998), Crustal structure above the Iceland mantle plume imaged by the ICEMELT refraction profile, *Geophys. J. Int.*, *135*, 1131–1149, doi:10.1046/j.1365-246X.1998.00701.x.

Darbyshire, F. A., K. F. Priestley, R. S. White, R. Stefánsson, G. B. Gudmundsson, and S. S. Jakobsdóttir (2000), Crustal structure of central and northern Iceland from analysis of teleseismic receiver functions, *Geophys. J. Int.*, *143*, 163–184, doi:10.1046/j.1365-246x.2000.00224.x.

Dasgupta, R., and M. M. Hirschmann (2006), Melting in Earth's deep upper mantle caused by carbon dioxide, *Nature*, *440*, 659–662, doi:10.1038/nature04612.

Elliott, T. R., C. J. Hawkesworth, and K. Grönvold (1991), Dynamic melting of the Iceland plume, *Nature*, *351*, 201–206, doi:10.1038/351201a0.

Foulger, G. R., and D. L. Anderson (2005), A cool model for the Iceland hotspot, *J. Volcanol. Geotherm. Res.*, *141*, 1–22, doi:10.1016/j.jvolgeores.2004.10.007.

Hardarson, B. S., J. G. Fitton, R. M. Ellam, and M. S. Pringle (1997), Rift relocation—A geochemical and geochronological investigation of a palaeo-rift in northwest Iceland, *Earth Planet. Sci. Lett.*, *153*, 181–196, doi:10.1016/S0012-821X(97)00145-3.

Heinonen, J. S., E. S. Jennings, and T. R. Riley (2015), Crystallisation temperatures of the most Mg-rich magmas of the Karoo LIP on the basis of Al-in-olivine thermometry, *Chem. Geol.*, *411*, 26–35, doi:10.1016/j.chemgeo.2015.06.015.

Helz, R. T. (1987), Diverse olivine types in lava of the 1959 eruption of Kilauea volcano and their bearing on eruption dynamics, *U.S. Geol. Surv. Prof. Pap.*, *1350*, 691–722.

Helz, R. T., and C. R. Thornber (1987), Geothermometry of Kilauea Iki lava lake, Hawaii, *Bull. Volcanol.*, *49*, 651–668, doi:10.1007/BF01080357.

Hémond, C., N. T. Arndt, U. Lichtenstein, A. W. Hofmann, N. Óskarsson, and S. Steinthorsson (1993), The heterogeneous Iceland plume: Nd-Sr-O isotopes and trace element constraints, *J. Geophys. Res.*, *98*, 15,833–15,850, doi:10.1029/93JB01093.

Herzberg, C. (2011), Basalts as temperature probes of Earth's mantle, *Geology*, *39*, 1179–1180, doi:10.1130/focus122011.1.

Herzberg, C., and P. D. Asimow (2015), PRIMELT3 MEGA.XLSM software for primary magma calculation: Peridotite primary magma MgO contents from the liquidus to the solidus, *Geochem. Geophys. Geosyst.*, *16*, 563–578, doi:10.1002/2014GC005631.

Herzberg, C., C. Vidito, and N. A. Starkey (2016), Nickel-cobalt contents of olivine record origin of mantle peridotite and related rocks, *Am. Mineral.*, *101*, 1952–1966, doi:10.2138/am-2016-5538.

Hirschmann, M. M., and E. M. Stolper (1996), A possible role for garnet pyroxenite in the origin of the "garnet signature" in MORB, *Contrib. Mineral. Petrol.*, *124*, 185–208, doi:10.1007/s004100050184.

Hoggard, M. J., N. White, and D. Al-Attar (2016), Global dynamic topography observations reveal limited influence of large-scale mantle flow, *Nat. Geosci.*, *9*, 456–463, doi:10.1038/ngeo2709.

Hole, M. J., and J. Millet (2016), Controls of mantle potential temperature and lithospheric thickness on magmatism in the North Atlantic Igneous Province, *J. Petrol.*, *57*, 417–436.

Ito, G., Y. Shen, G. Hirth, and C. J. Wolfe (1999), Mantle flow, melting, and dehydration of the Iceland mantle plume, *Earth Planet. Sci. Lett.*, *165*, 81–96, doi:10.1016/S0012-821X(98)00216-7.

Jenkins, J., S. Cottaar, R. S. White, and A. Deuss (2016), Depressed mantle discontinuities beneath Iceland: Evidence of a garnet controlled 660 km discontinuity?, *Earth Planet. Sci. Lett.*, *433*, 159–168, doi:10.1016/j.epsl.2015.10.053.

Jones, S. M., B. J. Murton, J. G. Fitton, N. J. White, J. Maclennan, and R. L. Walters (2014), A joint geochemical-geophysical record of time-dependent mantle convection south of Iceland, *Earth Planet. Sci. Lett.*, *386*, 86–97, doi:10.1016/j.epsl.2013.09.029.

Katz, R. F., and J. F. Rudge (2011), The energetics of melting fertile heterogeneities within the depleted mantle, *Geochem. Geophys. Geosyst.*, *12*, Q0AC16, doi:10.1029/2011GC003834.

Katz, R. F., M. Spiegelman, and C. H. Langmuir (2003), A new parameterization of hydrous mantle melting, *Geochem. Geophys. Geosyst.*, *4*(9), 1073, doi:10.1029/2002GC000433.

Keiding, J. K., R. B. Trumball, I. V. Veksler, and D. A. Jerram (2011), On the significance of ultra-magnesian olivines in basaltic rocks, *Geology*, *39*, 1095–1098, doi:10.1130/G32214.1.

Kogiso, T., K. Hirose, and E. Takahashi (1998), Melting experiments on homogeneous mixtures of peridotite and basalt: Application to the genesis of ocean island basalts, *Earth Planet. Sci. Lett.*, *162*, 45–61, doi:10.1016/S0012-821X(98)00156-3.

Kokfelt, T., K. Hoernle, F. Hauff, J. Fiebig, R. Werner, and G. Garbe-Schonberg (2006), Combined trace element and Pb-Nd-Sr-Os isotope evidence for recycled oceanic crust (upper and lower) in the Iceland mantle plume, *J. Petrol.*, *47*, 1705–1749, doi:10.1093/petrology/egl025.

Korenaga, J., P. B. Kelemen, and W. S. Holbrook (2002), Methods for resolving the origin of large igneous provinces from crustal seismology, *J. Geophys. Res.*, *107*(B9), 2178, doi:10.1029/2001JB001030.
Maaløe, S., and S. P. Jakobsson (1980), The PT phase relations of a primary oceanite from the Reykjanes peninsula, Iceland, *Lithos*, *13*, 237–246, doi:10.1016/0024-4937(80)90069-9.
Maclennan, J. (2008), Lead isotope variability in olivine-hosted melt inclusions from Iceland, *Geochim. Cosmochim. Acta*, *72*, 4159–4176, doi:10.1016/j.gca.2008.05.034.
Maclennan, J., D. McKenzie, and K. Gronvöld (2001), Plume-driven upwelling under central Iceland, *Earth Planet. Sci. Lett.*, *194*, 67–82, doi:10.1016/S0012-821X(01)00553-2.
Maclennan, J., D. McKenzie, F. Hilton, K. Gronvld, and N. Shimizu (2003), Geochemical variability in a single flow from northern Iceland, *J. Geophys. Res.*, *108*(B1), 2007, doi:10.1002/2014GC005264.
McGovern, P. J., and G. Schubert (1989), Thermal evolution of the Earth: Effects of volatile exchange between atmosphere and interior, *Earth Planet. Sci. Lett.*, *96*, 27–37, doi:10.1016/0012-821X(89)90121-0.
McKenzie, D., and R. K. O'Nions (1991), Partial melt distributions from inversion of rare earth element concentrations, *J. Petrol.*, *32*, 1021–1091, doi:10.1093/petrology/32.5.1021.
McKenzie, D. A. N. (1984), The generation and compaction of partially molten rock, *J. Petrol.*, *25*(3), 713–765, doi:10.1093/petrology/25.3.713.
Nicholson, H., M. Condomines, J. G. Fitton, A. E. Fallick, K. Grönvold, and G. Rogers (1991), Geochemical and isotopic evidence for crustal assimilation beneath Krafla, Iceland, *J. Petrol.*, *32*, 1005–1020, doi:10.1093/petrology/32.5.1005.
Óskarsson, N., Ö. Helgason, and S. Steinthórsson (1994), Oxidation state of iron in mantle-derived magmas of the Icelandic rift zone, *Hyperfine Interact.*, *91*, 733–737, doi:10.1007/BF02064599.
Peate, D. W., K. Breddam, J. A. Baker, M. D. Kurz, A. K. Barker, T. Prestvik, N. Grassineau, and A. C. Skovgaard (2010), Compositional characteristics and spatial distribution of enriched Icelandic mantle components, *J. Petrol.*, *51*, 1447–1475, doi:10.1093/petrology/egq025.
Pertermann, M., and M. M. Hirschmann (2003), Partial melting experiments on a MORB-like pyroxenite between 2 and 3 GPa: Constraints on the presence of pyroxenite in basalt source regions from solidus location and melting rate, *J. Geophys. Res.*, *108*(B2), 2125, doi:10.1029/2000JB000118.
Phipps Morgan, J. (2001), Thermodynamics of pressure release melting of a veined plum pudding mantle, *Geochem. Geophys. Geosyst.*, *2*(4), 1001, doi:10.1029/2000GC000049.
Putirka, K. D. (2005), Mantle potential temperatures at Hawaii, Iceland, and the mid-ocean ridge system, as inferred from olivine phenocrysts: Evidence for thermally driven mantle plumes, *Geochem. Geophys. Geosyst.*, *6*, Q05L08, doi:10.1029/2005GC000915.
Putirka, K. D. (2008a), Excess temperatures at ocean islands: Implications for mantle layering and convection, *Geology*, *36*, 283–286, doi:10.1130/G24615A.1.
Putirka, K. D. (2008b), Thermometers and barometers for volcanic systems, *Rev. Mineral. Geochem.*, *69*, 61–120, doi:10.2138/rmg.2008.69.3.
Putirka, K. D. (2016), Rates and style of planetary cooling on Earth, Moon, Mars and Vesta, using new models for oxygen fugacity, ferric-ferrous ratios, olivine-liquid Fe-Mg exchange, and mantle potential temperature, *Am. Mineral.*, *101*, 819–840, doi:10.2138/am-2016-5402.
Putirka, K. D., M. Perfit, F. J. Ryerson, and M. G. Jackson (2007), Ambient and excess mantle temperatures, olivine thermometry, and active vs. passive upwelling, *Chem. Geol.*, *241*, 177–206, doi:10.1016/j.chemgeo.2007.01.014.
Ribe, N. M., U. R. Christensen, and J. Theißing (1995), The dynamics of plume-ridge interaction, 1: Ridge-centered plumes, *Earth Planet. Sci. Lett.*, *134*, 155–168, doi:10.1016/0012-821X(95)00116-T.
Rickers, F., A. Fichtner, and J. Trampert (2013), The Iceland–Jan Mayen plume system and its impact on mantle dynamics in the North Atlantic Region: Evidence from full-waveform inversion, *Earth Planet. Sci. Lett.*, *367*, 39–51, doi:10.1016/j.epsl.2013.02.022.
Roeder, P. L., and R. F. Emslie (1970), Olivine-liquid equilibrium, *Contrib. Mineral. Petrol.*, *29*, 275–289, doi:10.1007/BF00371276.
Rudge, J. F., J. Maclennan, and A. Stracke (2013), The geochemical consequences of mixing melts from a heterogeneous mantle, *Geochim. Cosmochim. Acta*, *114*, 112–143, doi:10.1016/j.gca.2013.03.042.
Saemundsson, K. (1991), Geology of the Krafla system, in *The Natural History of Lake Myvatn*, pp. 24–95, The Icelandic Nat. History Soc., Reykjavik.
Shen, Y., et al. (2002), Seismic evidence for a tilted mantle plume and north-south mantle flow beneath Iceland, *Earth Planet. Sci. Lett.*, *197*, 261–272, doi:10.1016/S0012-821X(02)00494-6.
Shorttle, O., and J. Maclennan (2011), Compositional trends of Icelandic basalts: Implications for short-length scale lithological heterogeneity in mantle plumes, *Geochem. Geophys. Geosyst.*, *12*, Q11008, doi:10.1029/2011GC003748.
Shorttle, O., J. Maclennan, and S. M. Jones (2010), Control of the symmetry of plume-ridge interaction by spreading ridge geometry, *Geochem. Geophys. Geosyst.*, *11*, Q0AC05, doi:10.1029/2009GC002986.
Shorttle, O., J. Maclennan, and S. Lambart (2014), Quantifying lithological variability in the mantle, *Earth Planet. Sci. Lett.*, *395*, 24–40, doi:10.1016/j.epsl.2014.03.040.
Shorttle, O., Y. Moussallam, M. E. Hartley, J. Maclennan, M. Edmonds, and B. J. Murton (2015), Fe-XANES analyses of Reykjanes Ridge basalts: Implications for oceanic crust's role in the solid Earth oxygen cycle, *Earth Planet. Sci. Lett.*, *427*, 272–285, doi:10.1016/j.epsl.2015.07.017.
Sims, K. W. W., J. Maclennan, J. Blichert-Toft, E. M. Mervine, J. Bluszatajn, and K. Grönvold (2013), Short length scale mantle heterogeneity beneath Iceland probed by glacial modulation of melting, *Earth Planet. Sci. Lett.*, *379*, 146–157, doi:10.1016/j.epsl.2013.07.027.
Skovgaard, A. C., M. Storey, J. Baker, J. Blusztajn, and S. R. Hart (2001), Osmium–oxygen isotopic evidence for a recycled and strongly depleted component in the Iceland mantle plume, *Earth Planet. Sci. Lett.*, *194*, 259–275, doi:10.1016/S0012-821X(01)00549-0.
Slater, L., D. A. N. McKenzie, K. Grönvold, and N. Shimizu (2001), Melt generation and movement beneath Theistareykir, NE Iceland, *J. Petrol.*, *42*(2), 321–354, doi:10.1093/petrology/42.2.321.
Sleep, N. H. (1984), Tapping of magmas from ubiquitous mantle heterogeneities: An alternative to mantle plumes?, *J. Geophys. Res.*, *89*, 10,029–10,041, doi:10.1029/JB089iB12p10029.
Sobolev, A. V. (1996), Melt inclusions in minerals as a source of principle petrological information, *Petrology*, *4*(3), 209–220.
Sobolev, A. V., and N. Shimizu (1994), The origin of typical NMORB: The evidence from a melt inclusion study, *Mineral. Mag.*, *58A*, 862–863.
Sobolev, A. V., A. W. Hofmann, G. Brügmann, V. G. Batanova, and D. V. Kuzmin (2008), A quantitative link between recycling and osmium isotopes, *Science*, *321*, 536–536, doi:10.1126/science.1158452.
Spandler, C., and H. St C. O'Neill (2009), Diffusion and partition coefficients of minor and trace elements in San Carlos olivine at 1,300°C with some geochemical implications, *Contrib. Mineral. Petr.*, *159*, 791–818, doi:10.1007/s00410-009-0456-8.
Spice, H. E., J. G. Fitton, and L. A. Kirstein (2016), Temperature fluctuation of the Iceland mantle plume through time, *Geochem. Geophys. Geosyst.*, *17*, 243–254, doi:10.1002/2015GC006059.
Spiegelman, M., and P. B. Kelemen (2003), Extreme chemical variability as a consequence of channelized melt transport, *Geochem. Geophys. Geosyst.*, *4*(7), 1055, doi:10.1029/2002GC000336.

Stolper, E., and P. Asimow (2007), Insights into mantle melting from graphical analysis of one-component systems, *Am. J. Sci.*, *307*(8), 1051–1139, doi:10.2475/08.2007.01.

Stracke, A., M. Bizimis, and V. J. Salters (2003a), Recycling oceanic crust: Quantitative constraints, *Geochem. Geophys. Geosyst.*, *4*(3), 8003, doi:10.1029/2001GC000223.

Stracke, A., A. Zindler, V. J. Salters, D. McKenzie, and K. Grönvold (2003b), The dynamics of melting beneath Theistareykir, northern Iceland, *Geochem. Geophys. Geosyst.*, *4*(10), 8513, doi:10.1029/2002GC000347.

Thomson, A., and J. Maclennan (2013), The distribution of olivine compositions in Icelandic basalts and picrites, *J. Petrol.*, *54*, 745–768, doi:10.1093/petrology/egs083.

Walter, M. J. (1998), Melting of garnet peridotite and the origin of komatiite and depleted lithosphere, *J. Petrol.*, *39*, 29–60, doi:10.1093/petroj/39.1.29.

Wan, Z., L. A. Coogan, and C. Dante (2008), Experimental calibration of aluminum partitioning between olivine and spinel as a geothermometer, *Am. Mineral.*, *93*, 1142–1147, doi:10.2138/am.2008.2758.

Werner, R., H. U. Schmincke, and G. Sigvaldason (1996), A new model for the evolution of table mountains: Volcanological and petrological evidence from Herdubreid and Herdubreidartögl volcanoes (Iceland), *Geol. Rundsch.*, *85*(2), 390–397, doi:10.1007/BF02422244.

White, R., and D. McKenzie (1989), Magmatism at rift zones: The generation of volcanic continental margins and flood basalts, *J. Geophys. Res.*, *94*, 7685–7729, doi:10.1029/JB094iB06p07685.

White, R. S., D. McKenzie, and R. K. O'Nions (1992), Oceanic crustal thickness from seismic measurements and rare earth element inversions, *J. Geophys. Res.*, *97*, 19,683–19,715, doi:10.1029/92JB01749.

White, R. S., et al. (2008), Lower-crustal intrusion on the North Atlantic continental margin, *Nature*, *452*, 460–464, doi:10.1038/nature06687.

Winpenny, B., and J. Maclennan (2011), A partial record of mixing of mantle melts preserved in Icelandic phenocrysts, *J. Petrol.*, *52*, 1791–1812, doi:10.1093/petrology/egr031.

Wyllie, P. J. (1975), Influence of mantle CO_2 in the generation of carbonatites and kimberlites, *Nature*, *257*, 297–299, doi:10.1038/257297a0.